

Smoothing Variances Across Time: Adaptive Stochastic Volatility

Jason B. Cho*

Department of Statistics and Data Science, Cornell University
and

David S. Matteson

Department of Statistics and Data Science, Cornell University

December 25, 2024

Abstract

We introduce a novel Bayesian framework for estimating time-varying volatility by extending the Random Walk Stochastic Volatility (RWSV) model with a new Dynamic Shrinkage Process (DSP) in (log) variances. Unlike classical Stochastic Volatility or GARCH-type models with restrictive parametric stationarity assumptions, our proposed Adaptive Stochastic Volatility (ASV) model provides smooth yet dynamically adaptive estimates of evolving volatility and its uncertainty (vol of vol). We derive the theoretical properties of the proposed global-local shrinkage prior. Through simulation studies, we demonstrate that ASV exhibits remarkable misspecification resilience with low prediction error across various data generating scenarios in simulation. Furthermore, ASV's capacity to yield locally smooth and interpretable estimates facilitates a clearer understanding of underlying patterns and trends in volatility. Additionally, we show that this attribute makes ASV a robust tool applicable across a wide range of disciplines, including in finance, environmental science, epidemiology, and medicine, among others.

Keywords: Time series; Trend filtering; Dynamic linear model;

*The authors gratefully acknowledge financial support from *National Science Foundation grants OAC-1940124 and DMS-2114143*

1 Introduction

Volatility in a time series measures deviations from its average, providing insights into the data-generating process. Estimating volatility holds significant importance across diverse fields as it offers crucial insights into the underlying data generating process. In finance, volatility estimation is crucial for pricing, risk assessment, and asset management. In epidemiology, it aids in early outbreak detection and forecasting new cases of diseases Kostoulas et al. [2021], Achcar et al. [2020], Sarkar and Chatterjee [2017]. Climate science uses time-varying volatility models to study phenomena like tornadoes, droughts, and rainfall Tippett [2014], Modarres and Ouarda [2014], Mehdizadeh et al. [2017]. In engineering, volatility helps predict mechanical failures Pham and Yang [2010], Ma et al. [2017], while in hydrology, it informs understanding of streamflow variations Wang et al. [2005, 2023a,b], Otache [2012].

Existing models for volatility estimation, such as the Autoregressive Conditional Heteroskedasticity (ARCH) model [Engle, 1982], the Generalized ARCH (GARCH) model [Bollerslev, 1986], and the Stochastic Volatility (SV) model [Hull and White, 1987, Taylor, 2008, Melino and Turnbull, 1990], assume stationarity. This assumption often leads to inaccuracies, particularly when the volatility process experiences gradual or abrupt shifts. Empirical evidence across disciplines points to evolving volatility patterns driven by factors like market dynamics Chou [1988], French et al. [1987], Poon and Taylor [1992], So et al. [1997], Su and Wang [2020], Nishino and Kakamu [2015], climate change Tippett [2014], and seasonal or outbreak-related effects in epidemiology Kostoulas et al. [2021]. These findings highlight the need for a flexible framework that can adaptively estimate volatility, accommodating both smooth and sudden changes.

A common approach to accommodate changing volatility is to introduce time-varying parameters through latent Markov switching models [Brunetti et al., 2008, Ardia et al., 2018]. In this framework, parameters are assumed to shift across a fixed number of latent regimes, with transitions governed by a hidden Markov process. This approach has been incorporated into ARCH, GARCH, and SV models Hamilton and Susmel [1994], Cai [1994], Bauwens et al. [2010], Gray [1996a], So et al. [1998], Hwang et al. [2004], offering increased flexibility. However, estimation of Markov Switching models is complex and inefficient (Gray [1996b], Billio et al. [2016]) as it requires identification of the latent regimes at each time point and the transition probabilities between them. Herein, we present the Adaptive Stochastic Volatility (ASV) model, building upon the Random Walk Stochastic Volatility (RWSV) (Ruiz [1994], Harvey et al. [1994]). RWSV assumes the log-variance of the observed process follows a Gaussian random walk with a constant variance. In contrast, ASV introduces two significant modifications to RWSV: it incorporates a time-varying variance for the log-variance increments and adopts a global-local shrinkage prior for adaptability.

We specifically highlight a class of global-local shrinkage prior called Dynamic Shrinkage Processes (DSP) [Kowal et al., 2019], which includes dynamic versions of a horseshoe prior [Carvalho et al., 2010] as a special case. DSP has shown versatility across various applications. For example, Wu et al. [2024a] integrates DSP into a Bayesian dynamic linear model to estimate change points and score outliers. Another application is seen in Schafer and Matteson [2024], where DSP is used to propose the negative binomial Bayesian trend filter (NB-BTF) for adaptively smoothing integer-valued time series. Additionally, Wu et al. [2024b] combines the Bayesian trend filter with DSP and machine learning-based regularization method to effectively distinguish micro-level drifts from macro-level shifts.

The standout feature of our proposed model, ASV, is its local adaptability, effectively estimating volatility in the presence of gradual or abrupt changes in the volatility process with notable smoothness in between. It allows robustness against model misspecification, resulting in low prediction errors across diverse data-generating scenarios. In addition, ASV’s volatility estimates exhibit smoother trajectories compared to those generated by alternative time-varying parameter models. The reduction in noise within our estimates provides users with clearer insights into underlying patterns and trends in the data.

Section 2 introduces our proposed models and their associated parameters; theoretical properties of DSP in comparison to other shrinkage priors are explored. Section 3 provides an overview of the Gibbs sampling scheme; Full conditional distributions are detailed in the supplementary material. Comparisons between proposed models on simulated data are presented in Section 4. Subsequently, Section 5 presents empirical analyses of three datasets: weekly log-returns on the S&P 500 index, weekly log-returns on EURO/USD exchange rate and weekly changes in death tolls from COVID-19 in the U.S. based on the proposed method. In Section 6, Bayesian Trend Filter with Adaptive Stochastic Volatility (BTF-ASV), which simultaneously estimates the time-varying means and the variances, is applied to the surface air temperature anomaly data for empirical analysis.

2 Methodology

2.1 The Random Walk Stochastic Volatility Model

Adaptive Stochastic Volatility (ASV) may be viewed as an extension of Random Walk Stochastic Volatility (RWSV) model (Ruiz [1994], Harvey et al. [1994]). Consider a zero mean process with T observations, $\{y_t\}_{t=1}^T$, and its log-variance term $\{h_t\}_{t=1}^T$. Stochastic

Volatility (SV) model assumes the observed process y_t to follow a normal distribution with its log-variance term, h_t , following the lag order 1 autoregression. RWSV is a special case of SV model where the autoregressive coefficient is assumed to be 1. Thus, the model is defined as:

$$y_t = \exp\{h_t/2\}\epsilon_t \quad \epsilon_t \stackrel{iid}{\sim} N(0, 1)$$

$$\Delta h_t := h_t - h_{t-1} = \sigma_h u_t \quad u_t \stackrel{iid}{\sim} N(0, 1).$$

In RWSV, h_t is governed by a time-invariant variance term, σ_h^2 , which determines the degree of variation between successive log-variances. A large σ_h^2 implies high probability of significant changes in the h_t process, whereas a small σ_h^2 indicates high probability of minimal to no changes in h_t . In a frequentist framework, σ_h is typically treated as a fixed parameter, often estimated via Quasi-Maximum Likelihood, as demonstrated in the original papers by Ruiz [1994] and Harvey et al. [1994]. More recent studies, such as that by Nishino and Kakamu [2015], have employed a Bayesian framework for estimation with a non-informative prior on σ_h^2 .

2.2 Stochastic Volatility with Local Only Shrinkage

RWSV model, however, may provide a poor fit for time series exhibiting both significant and minimal changes due to its assumption of a time-invariant σ_h^2 . Ideally, we prefer σ_h^2 to be time-varying, remaining small during periods of little to no significant changes and increasing to a large value during periods of abrupt changes in h_t . A frequentist approach to addressing this problem would be by imposing an additional penalty term like the l_1 penalty (Tibshirani [1996]). Similarly in Bayesian setting, sparsity inducing priors may be imposed on the parameters. Drawing from Bayesian representations of LASSO as discussed

in Park and Casella [2008] and the scale-mixture Gaussian representation of the Laplace distribution in West [1987], we propose an intermediary model called RWSV with Bayesian LASSO (RWSV-BL), which incorporates a time-varying variance for h_t as

$$\Delta h_t \sim N(0, \sigma_{h,t}^2) \quad \sigma_{h,t}^2 \stackrel{iid}{\sim} \text{Exp}\{(2\Lambda^2)^{-1}\}.$$

Under this Bayesian representation, Δh_t follows a normal distribution with one time-varying local parameter $\sigma_{h,t}^2$. RWSV-BL shares similarities with the $l1$ -trend filter proposed by Kim et al. [2009] and Tibshirani [2014], which aims to provide a smooth estimate of the observed process y_t . The key distinction between the $l1$ -trend filter and RWSV-BL lies in their respective focuses: while the $l1$ -trend filter targets the estimation of the time-varying mean of the process, RWSV-BL is designed to estimate the time-varying log-variance, h_t instead. Drawing an analogy between the trend-filter and RWSV-BL allows us to conceptualize our problem as a smoothing task applied to the variance process. By incorporating shrinkage priors on the higher-order differences of the log-variance process, the model can achieve greater smoothing on h_t .

2.3 Adaptive Stochastic Volatility via Global-Local Shrinkage

Building upon the model in the previous subsection, we propose the Adaptive Stochastic Volatility (ASV) model. Unlike RWSV-BL, which consists of a time-varying local parameter, ASV features a global-local structure for the variance of the log-variance, $\sigma_{h,t}^2$. Specifically, $\sigma_{h,t}$ is defined as $\sigma_{h,t} := \tau \lambda_t$, where τ represents the global parameter, and λ_t represents the local parameter. The global parameter τ controls the overall shrinkage and acts as the average shrinkage applied across all time points, while the local parameter λ_t controls smoothness at each time t in addition to τ . The inclusion of the global param-

eter τ enhances model smoothness by providing a consistent level of shrinkage across all time points, which we find as essential in the application and simulations sections below. In contrast, the Bayesian LASSO model, as discussed in section 2.2 only incorporates a local parameter for $\sigma_{h,t}^2$. Section 5 shows ASV to yield significantly smoother estimates of h_t compared to RWSV-BL. Therefore, we propose the following model for estimating time-varying volatility:

$$\Delta^k h_t \sim N(0, \tau^2 \lambda_t^2) \quad \tau \sim \pi(\tau), \quad \lambda_t \stackrel{iid}{\sim} \pi(\lambda_t),$$

where k is usually set to 1 or 2, and $\pi(\tau)$ and $\pi(\lambda_t)$ represent priors on τ and λ_t . Global-local shrinkage priors for Gaussian observations have been extensively studied in the past decade, particularly in the context of high-dimensional regression. Examples of such priors include the Horseshoe prior by Carvalho et al. [2010], the Horseshoe plus prior by Bhadra et al. [2015], the triple gamma prior by Cadonna et al. [2019], and Dynamic Shrinkage Processes (DSP) introduced by Kowal et al. [2019]. The global parameter, τ , ensures that the estimate of h_t remains smooth overall, while the local parameter, λ_t , allows for local adaptivity in the presence of abrupt changes. Among the various aforementioned global-local priors, DSP are further analyzed and incorporated into the ASV model in this work. Two versions of ASV are explored: Adaptive Stochastic Volatility with Dynamic Horseshoe Prior (ASV-DHS) and Adaptive Stochastic Volatility with Horseshoe Prior (ASV-HP), the latter of which can be considered a special case of ASV-DHS.

2.4 Properties of Dynamic Shrinkage Processes

DSP distinguish themselves among global-local priors by incorporating temporal dependence in the local shrinkage parameter λ_t , allowing for a dynamic shrinkage approach.

Kowal et al. [2019] applied DSP in Bayesian trend filtering and demonstrated its superior performance in terms of prediction error when estimating the mean of an arbitrary time series, compared to other well-studied horseshoe prior. Therefore, we focus on DSP as the prior distribution on h_t . Under this framework, $h_t \sim N(0, \sigma_{h,t}^2)$ and the priors on $\sigma_{h,t}$ are defined by its log-squared term, $v_t := \log(\sigma_{h,t}^2)$:

$$v_t = \mu + \psi_t + \eta_t \quad \eta_t \stackrel{iid}{\sim} Z(a, b, 0, 1),$$

where Z -distribution has the following density function (Barndorff-Nielsen et al. [1982]):

$$f(z|a, b, \mu_z, \sigma_z) = (\sigma_z \beta(a, b))^{-1} \left(\exp\left\{ \frac{z - \mu_z}{\sigma_z} \right\} \right)^a \left(1 + \exp\left\{ \frac{z - \mu_z}{\sigma_z} \right\} \right)^{-(a+b)}.$$

For the global parameter, $\tau = \exp\{\mu/2\}$ and $\lambda_t = \exp\{(\psi_t + \eta_t)/2\}$ represents the local parameter. Specifically, ψ_t models the temporal dependence of the process. A few candidate models for ψ_t includes the Hidden Markov Models, linear regression, or spline. For simplicity, the serial dependence is assumed to be positive, indicating that large $\sigma_{h,t}^2$ is likely to result in large $\sigma_{h,t+1}^2$. Heuristic interpretation of this assumption is that large changes is likely to be followed by another large changes, while small changes is likely to be followed by small changes. Thus, $\psi_t := \phi(v_t - \mu)$, with $\eta_t \sim Z(a, b, 0, 1)$ corresponding to the i.i.d scale parameter. The benefit of having Z -distribution as prior on η_t is its shrinkage property. By setting $a = b = 1/2$ and $\phi = 0$, we have the horseshoe prior (Carvalho et al. [2010]), as $\lambda_t = \exp\{\eta_t/2\} \sim C^+(0, 1)$ is equivalent to $\eta_t \sim Z(1/2, 1/2, 0, 1)$.

Owing to its autoregressive structure, the shrinkage profile of DSP is analyzed conditional on either the previous shrinkage term $\kappa_t := \frac{1}{1 + \exp\{v_t\}}$ or the local scale parameter λ_t , which both follow Three Parameter Beta distribution (Kowal et al. [2019]). We consider

the shrinkage profile of the stationary distribution of v_t . We show that DSP has similar properties as Horseshoe prior but induces heavier shrinkage. Let's first define $z_{t,h} := \phi^h \eta_{t-h}$. Infinite order Moving Average representation of v_t results in:

$$\begin{aligned} v_t &= \mu + \phi(v_{t-1} - \mu) + \eta_t & \eta_t &\sim Z(1/2, 1/2, 0, 1) \\ &= \mu + \sum_{h=0}^{\infty} \phi^h \eta_{t-h} \\ &= \mu + \sum_{h=0}^{\infty} z_{t,h}. \end{aligned}$$

As shown in Barndorff-Nielsen et al. [1982], $z_{t,h}$ is a scaled Hyperbolic Secant Distribution, with $E(z_{t,h}|\phi) = 0$ and $Var(z_{t,h}|\phi) = (|\phi|^h \pi)^2$. Let's consider $z_t := \sum_{h=0}^{\infty} z_{t,h}$.

Theorem 1. z_t converges almost surely if and only if $|\phi| < 1$.

Proof. This directly follows from Kolmogorov's three series theorem. Note that the variance $\sum_{h=0}^{\infty} var(z_{t,h}|\phi)$ converges if and only if $|\phi| < 1$. Exact derivation is explored in Appendix A.1. □

Corollary 1.1. When $|\phi| < 1$,

$$\begin{aligned} E(z_t|\phi) &= E\left(\sum_{h=0}^{\infty} z_{t,h}|\phi\right) = \sum_{h=0}^{\infty} E(z_{t,h}|\phi) = 0 \\ var(z_t|\phi) &= var\left(\sum_{h=0}^{\infty} z_h|\phi\right) = \sum_{h=0}^{\infty} var(z_h|\phi) = \sum_{h=0}^{\infty} \pi^2 \phi^{2h} = \frac{\pi^2}{1 - \phi^2} \end{aligned}$$

Characteristic function of $z_{h,t}$ is $sech(\pi\phi^h t)$. Thus, the characteristic function, $g(t)$, for $\sum_{h=0}^{\infty} z_{h,t}$, would be an infinite product of the characteristic function of $z_{h,t}$.

$$g(t) = \prod_{h=0}^{\infty} sech(\pi\phi^h t) \qquad -\frac{1}{2} < t < \frac{1}{2}$$

Similarly, for the Moment Generating function $M(t)$

$$M(t) = \prod_{h=0}^{\infty} \sec(\pi\phi^h t) \quad -\frac{1}{2} < t < \frac{1}{2}$$

Theorem 2. If $|\phi| = 0.5$, $\eta_{t-h} \stackrel{iid}{\sim} Z(1/2, 1/2, 0, 1)$, and $z_{t,h} := \phi^h \eta_{t-h}$, then $z_t := \sum_{h=0}^{\infty} z_{t,h} \xrightarrow{a.s.} \text{Logistic}(0, 2)$.

Proof. Derivations are explored in Appendix A.2. □

Thus, assuming $\mu = 0$ and $\phi = 0.5$ for simplicity, we have the following density function for v_t , $\lambda_t := \exp\{v_t/2\}$ and $\kappa_t := \frac{1}{1+\exp\{v_t\}}$ for the stationary distribution of DSP:

$$\begin{aligned} f(v_t) &= \frac{1}{8} \text{sech}^2\left(\frac{v_t}{4}\right) \\ f(\lambda_t) &= \frac{1}{4\lambda_t} \text{sech}^2\left(\frac{\log(\lambda_t)}{2}\right) = \frac{1}{(1+\lambda_t)^2} \\ f(\kappa_t) &= \frac{1}{8(\kappa_t)(1-\kappa_t)} \text{sech}^2\left(\frac{1}{4}\left(\log\left(\frac{1-\kappa_t}{\kappa_t}\right)\right)\right) = \frac{1}{\sqrt{\kappa_t(1-\kappa_t)}} \frac{1}{2\kappa_t(1+\sqrt{\frac{1-\kappa_t}{\kappa_t}})^2}. \end{aligned}$$

Figure 2.4 compares the prior distribution of λ_t and κ_t for the Horseshoe and DSP. Let's

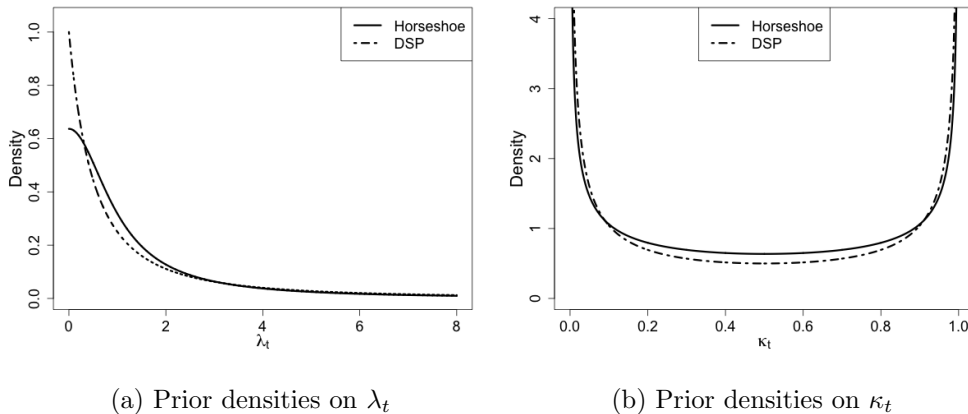


Figure 1: Comparisons of prior densities on λ_t and κ_t between Horseshoe Prior and the stationary distribution of Dynamic Shrinkage Process (DSP) with $\eta_t \stackrel{iid}{\sim} Z(1/2, 1/2, 0, 1)$, $\phi = 1/2$ and $\mu = 0$.

remind ourselves that the Horseshoe prior in Carvalho et al. [2010] assumes $\lambda_t \sim C^+(0, 1)$

and $\kappa_t \sim \text{Beta}(1/2, 1/2)$. The density function for Horseshoe, $g(\lambda_t)$ and $g(\kappa_t)$ are:

$$g(\lambda_t) = \frac{2}{\pi(1 + \lambda_t^2)} \qquad g(\kappa_t) = \frac{1}{\pi\sqrt{\kappa_t(1 - \kappa_t)}}.$$

For λ_t , the density function for DSP puts more weights as $\lambda_t \rightarrow 0$ and $\lambda_t \rightarrow \infty$. Specifically, $f(\lambda_t) > g(\lambda_t)$ when $\lambda_t \in (0, \frac{2 - \sqrt{(4 - \pi)\pi}}{(\pi - 2)}) \cup (\frac{2 + \sqrt{(4 - \pi)\pi}}{(\pi - 2)}, \infty)$. In terms of κ_t , the DSP puts more weight around 0 and 1 than Horseshoe. This is due to the extra U-shaped term in κ_t , $\frac{1}{2\kappa_t(1 + \sqrt{\frac{1 - \kappa_t}{\kappa_t}})^2}$, pushing the mass of the distribution to near 0 and 1. Let's consider the marginal density on Δh .

Theorem 3. Let $|\phi| = 0.5$, $\eta_{t-h} \stackrel{iid}{\sim} Z(1/2, 1/2, 0, 1)$, $z_{t,h} := \phi^h \eta_{t-h}$, $v_t := \sum_{h=0}^{\infty} z_{t,h}$, $\lambda_t := \exp\{v_t/2\}$ and $\Delta h_t \sim N(0, \lambda_t)$,

$$\begin{aligned} \lim_{\Delta h_t \rightarrow 0} f(\Delta h_t) &= \infty \\ K_L \log\left(1 + \frac{4}{\Delta^2 h_t}\right) &< f(\Delta h_t) < K_U \log\left(1 + \frac{2}{\Delta^2 h_t}\right), \quad |\Delta h_t| > 0 \end{aligned}$$

where $K_U = \frac{1}{2\sqrt{2\pi}}$ and $K_L = \frac{1}{8\sqrt{2\pi}}$

Proof. The proof is similar to Theorem 1 in Carvalho et al. [2010]. We use the fact that $\forall x > 0$,

$$\frac{1}{2(1 + x^2)} \leq \frac{1}{(1 + x)^2} \leq \frac{1}{(1 + x^2)}$$

Derivation is detailed in Appendix A.3. □

The bounds for the marginal distribution of DSP are similar to the ones from the Horseshoe with the only difference being the constant factor K_L and K_U . Under Horseshoe, $K_U = \frac{1}{\sqrt{2\pi^3}}$ and $K_L = \frac{1}{2\sqrt{2\pi^3}}$. Like horseshoe prior, DSP is also unbounded near the origin, which leads to super-efficiency in a sparse setting as shown in Carvalho et al. [2010].

2.5 Modeling Trends in Both Mean and Variance

Finally, we propose Bayesian Trend Filter with Adaptive Stochastic Volatility (BTF-ASV) by combining Bayesian Trend Filter with Dynamic Horseshoe Process (BTF-DHP) proposed in Kowal et al. [2019] and ASV model proposed in this paper. BTF-ASV is able to generate smooth and locally adaptive estimate of the time varying mean parameter β_t through the Bayesian Trend Filter, and the time varying log variance parameter h_t via ASV, simultaneously.

Let's define $\omega_{\beta,t} := \Delta^k \beta_t$ and also similarly define for variables $v_{\beta,t}, u_{\beta,t}, \mu_{\beta}, \phi_{\beta}, \eta_{\beta,t}$ as well as for hyper-parameters $a_{\eta_{\beta}}, b_{\eta_{\beta}}, a_{\mu_{\beta}}, b_{\mu_{\beta}}, a_{\phi_{\beta}}, b_{\phi_{\beta}}$. We have the following Bayesian hierarchical representation of BTF-ASV:

$$y_t = \beta_t + \exp\{h_t/2\}\epsilon_t \quad \epsilon_t \stackrel{iid}{\sim} N(0, 1) \quad (1a)$$

$$\Delta^k \beta_t = \omega_{\beta,t} = \exp\{v_{\beta,t}/2\}u_{\beta,t} \quad u_{\beta,t} \stackrel{iid}{\sim} N(0, 1) \quad (1b)$$

$$v_{\beta,t+1} = \mu_{\beta} + \phi_{\beta}(v_{\beta,t} - \mu_{\beta}) + \eta_{\beta,t} \quad \eta_{\beta,t} \stackrel{iid}{\sim} Z(a_{\eta_{\beta}}, b_{\eta_{\beta}}, 0, 1) \quad (1c)$$

$$\mu_{\beta} \sim Z(a_{\mu_{\beta}}, b_{\mu_{\beta}}, 0, 1) \quad (\phi_{\beta} + 1)/2 \sim \text{Beta}(a_{\phi_{\beta}}, b_{\phi_{\beta}}) \quad (1d)$$

$$\Delta^k h_t = \omega_{h,t} = \exp\{v_{h,t}/2\}u_{h,t} \quad u_{h,t} \stackrel{iid}{\sim} N(0, 1) \quad (1e)$$

$$v_{h,t+1} = \mu_h + \phi_h(v_{h,t} - \mu_h) + \eta_{h,t} \quad \eta_{h,t} \stackrel{iid}{\sim} Z(a_{\eta_h}, b_{\eta_h}, 0, 1) \quad (1f)$$

$$\mu_h \sim Z(a_{\mu_h}, b_{\mu_h}, 0, 1) \quad (\phi_h + 1)/2 \sim \text{Beta}(a_{\phi_h}, b_{\phi_h}) \quad (1g)$$

Line 1a represents the observation equation, lines 1b through 1d specify the priors on the time varying mean, β_t and lines 1e through 1g specify the priors on the time varying log-variance, h_t . Application of BTF-ASV is explored in Section 6.

3 Parameter Estimation via Gibbs Sampling

Let's remind ourselves that ASV has the following hierarchical representation:

$$y_t = \exp\{h_t/2\}\epsilon_t \quad \epsilon_t \stackrel{iid}{\sim} N(0, 1) \quad (2a)$$

$$\Delta^k h_t = \omega_t = \exp\{v_t/2\}u_t \quad u_t \stackrel{iid}{\sim} N(0, 1) \quad (2b)$$

$$v_{t+1} = \mu + \phi(v_t - \mu) + \eta_t \quad \eta_t \stackrel{iid}{\sim} Z(a_\eta, b_\eta, 0, 1). \quad (2c)$$

$$\mu \sim Z(a_\mu, a_\mu, 0, 1) \quad (\phi + 1)/2 \sim \text{Beta}(a_\phi, b_\phi), \quad (2d)$$

where $a_\eta, b_\eta, a_\mu, a_\mu, a_\phi$, and b_ϕ are hyperparameters. Define $\mathbf{y} := (y_1, \dots, y_T)'$, $\mathbf{h} := (h_1, \dots, h_T)'$, and $\mathbf{v} := (v_1, \dots, v_T)'$. The goal is to sample from the posterior distribution, $f(\mathbf{h}, \mathbf{v}, \mu, \phi | \mathbf{y})$. This may be achieved using Gibbs sampling, in which full conditional distribution for each variables, \mathbf{h} , \mathbf{v} , μ , and ϕ are sampled sequentially.

Estimating h_t in the SV model is challenging due to its non-linear likelihood dependence. While methods like Sequential Monte Carlo Jacquier et al. [1994] sample h_t sequentially given past and future values, this is computationally demanding. Instead, we use a quasi-likelihood approach based on $y_t^* := \log(y_t^2)$ and $\mathbf{y}^* := (y_1^*, \dots, y_T^*)'$, transforming the model into a linear system with a non-Gaussian error term. This term is approximated by a Gaussian mixture distribution Kim et al. [1998], Omori et al. [2007]. Specifically, the 10-component Gaussian mixture by Omori et al. [2007] is used to approximate ϵ_t^* ; the exact distribution for π is detailed in Omori et al. [2007]:

$$y_t^* = h_t + \log(\epsilon_t^2), \quad \epsilon_t \stackrel{iid}{\sim} N(0, 1),$$

$$y_t^* \approx h_t + \mu_{j_t} + \sigma_{j_t} o_t, \quad o_t \stackrel{iid}{\sim} N(0, 1), \quad j_t \stackrel{iid}{\sim} \text{Categorical}(\pi).$$

The same approximation and parameter expansion on y^* is then applied to \mathbf{v} , as $\log(\boldsymbol{\omega}^2) = \mathbf{v} + \log(\mathbf{u}^2)$. The same 10-component Gaussian mixture by Omori et al. [2007], s , is introduced. Let's direct our attention to Lines 2c and 2d of Model 3, which can be interpreted as a Stochastic Volatility (SV) model with a heavy tailed error distribution $\eta_t \sim Z(a_\eta, b_\eta, 0, 1)$. Leveraging the mean-variance scale mixture representation of the Z -distribution Barndorff-Nielsen et al. [1982], we introduce additional parameters to facilitate efficient sampling. Sampling from the Pólya-Gamma random variable is performed by truncating an infinite sum, as proposed by Polson et al. [2013]. With parameter expansion, we can employ the efficient AWOL sampler by Kastner and Frühwirth-Schnatter [2014] to sample \mathbf{v} , μ , and ϕ . With parameters introduced, we have the following representation of the same model:

$$\begin{aligned}
y_t^* &\approx h_t + \mu_{j_t} + \sigma_{j_t} o_t & o_t &\stackrel{iid}{\sim} N(0, 1) \\
\Delta^k h_t = \omega_t^* &\approx v_t + \mu_{s_t} + \sigma_{s_t} r_t & r_t &\stackrel{iid}{\sim} N(0, 1) \\
v_{t+1} &= \xi_\mu^{-1/2} \mu + \phi(v_t - \mu) + \xi_t^{-1/2} \eta_t & \eta_t &\stackrel{iid}{\sim} N(0, 1) \\
\mu &\sim N(0, 1) & \xi_\mu &\stackrel{iid}{\sim} PG(1, 0) \\
\xi_t &\stackrel{iid}{\sim} N(0, 1) & s_t &\stackrel{iid}{\sim} Categorical(\boldsymbol{\pi}) \\
j_t &\stackrel{iid}{\sim} Categorical(\boldsymbol{\pi}) & (\phi + 1)/2 &\sim Beta(a_\phi, b_\phi).
\end{aligned}$$

In addition to the four parameters in the original equation, \mathbf{h} , \mathbf{v} , μ , and ϕ , four additional parameters, $\mathbf{j} := (j_1, \dots, j_T)'$, $\mathbf{s} := (s_1, \dots, s_T)'$, $\boldsymbol{\xi} := (\xi_1 \dots \xi_T)'$, and ξ_μ are introduced via parameter expansion and approximation. The detailed derivations of the conditional posterior distributions of each parameters are detailed in Appendix.

4 Simulation Study

4.1 Set-up

DGS1: SV with 1 Regime	DGS4: GARCH with 1 Regime
$h_{t+1} = 3 + 0.8(h_t - 3) + 0.2u_t$	$\sigma_{t+1}^2 = 1 + 0.1y_t^2 + 0.5\sigma_t^2$
DGS2: SV with 2 Regimes	DGS5: GARCH with 2 Regimes
$h_{t+1} = m_{s_{t+1}} + 0.8(h_t - m_{s_t}) + 0.2u_t$ $m_{s_t} = \begin{cases} -10, & \text{if } s_t = 0. \\ 6, & \text{if } s_t = 1. \end{cases}$	$\sigma_{t+1}^2 = m_{s_{t+1}} + 0.15y_t^2 + \beta_{s_{t+1}}\sigma_t^2$ $m_{s_t} = \begin{cases} 8, & \text{if } s_t = 0. \\ 0.1, & \text{if } s_t = 1. \end{cases}$ $\beta_{s_{t+1}} = \begin{cases} 0.8, & \text{if } s_t = 0. \\ 0.3, & \text{if } s_t = 1. \end{cases}$
DGS3: SV with 3 Regimes	DGS6: GARCH with 3 Regimes
$h_{t+1} = m_{s_{t+1}} + 0.8(h_t - m_{s_t}) + 0.2u_t$ $m_{s_t} = \begin{cases} -10, & \text{if } s_t = 0. \\ -3, & \text{if } s_t = 1. \\ 3, & \text{if } s_t = 2. \end{cases}$	$\sigma_{t+1}^2 = m_{s_{t+1}} + 0.15y_t^2 + \beta_{s_{t+1}}\sigma_t^2$ $m_{s_t} = \begin{cases} 12, & \text{if } s_t = 0. \\ 8, & \text{if } s_t = 1. \\ 0.1, & \text{if } s_t = 2. \end{cases}$ $\beta_{s_{t+1}} = \begin{cases} 0.8, & \text{if } s_t = 0. \\ 0.5, & \text{if } s_t = 1. \\ 0.2, & \text{if } s_t = 2. \end{cases}$

Table 1: Detailed summary of Data Generating Schemes (DGS) for the simulation study. Define $y_t = \sigma_t \epsilon_t$, $\epsilon_t \stackrel{iid}{\sim} N(0,1)$, $u_t \stackrel{iid}{\sim} N(0,1)$, $h_t := \log(\sigma_t^2)$. Sample paths were generated from the stochastic volatility model with 1, 2, and 3 regimes for DGS 1, 2, and 3, respectively, and from the GARCH model with 1, 2, and 3 regimes for DGS 4, 5, and 6, respectively. Transitions between states 0 and 1 for DGS 2 and DGS 4 are governed by the following transition matrix $\begin{pmatrix} 0.98 & 0.02 \\ 0.02 & 0.98 \end{pmatrix}$. Transitions between states 0, 1 and 2 for DGS 3 and DGS 6 are governed by $\begin{pmatrix} 0.98 & 0.01 & 0.01 \\ 0.01 & 0.98 & 0.01 \\ 0.01 & 0.01 & 0.98 \end{pmatrix}$. Each DGS comprises 1,000 sample paths, each path being 1,000 data points in length. Parameters for each DGS are detailed above.

The simulation study evaluates the performance of the proposed ASV model in comparison with established models: SV, MSSV, RWSV, GARCH, and MSGARCH. The com-

parison focuses on both accuracy of the mean estimate and the quality of uncertainty quantification. Specifically, we assess each model using three metrics: Mean Absolute Error (MAE), Empirical Coverage (EC), and Mean Credible Interval Width (MCIW):

$$MAE = \frac{1}{T} \sum_{t=1}^T |\sigma_t - \hat{\sigma}_t|, \quad EC = \frac{1}{T} \sum_{t=1}^T 1_{(\hat{\sigma}_{t,0.05}, \hat{\sigma}_{t,0.95})}(\sigma_t), \quad MCIW = \frac{1}{T} \sum_{t=1}^T (\hat{\sigma}_{t,0.95} - \hat{\sigma}_{t,0.05}).$$

The MAE measures the accuracy of the volatility estimate by calculating the average absolute difference between the true volatility σ_t and the model's estimate $\hat{\sigma}_t$. For Frequentist methods, the point estimate is based on maximum likelihood, while Bayesian methods use the posterior mean. The EC metric assesses the reliability of each model's uncertainty quantification by calculating the proportion of time points at which the true volatility falls within the model's 90% credible interval. Finally, the MCIW evaluates the precision of the uncertainty quantification, where a narrower credible interval represents a higher level of precision.

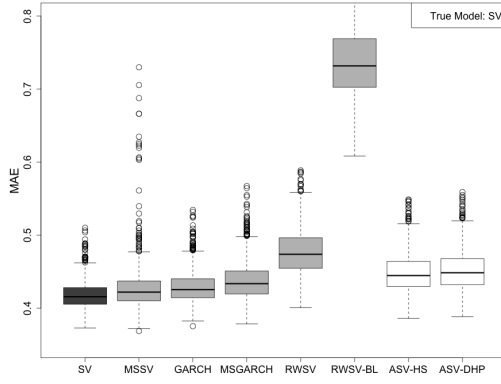
All models are implemented in R language R Core Team [2013]. Specifically, SV model is implemented via `stochvol` Kastner [2016] package, MSSV2 as specified in Hamilton [1989] and RWSV are implemented by the authors as no readily available packages in R exists. GARCH(1,1) models are fitted via `fGarch` Wuertz et al. [2023] package, and MSSV2 are fitted via `MSGARCH` (Ardia et al. [2019]) package. For fitting RWSV-BL, `dsp` package by Kowal et al. [2019] and `genlasso` package by Arnold and Tibshirani [2022] are used. `dsp` package by Kowal et al. [2019] is further expanded to implement ASV models. For all Bayesian models, 5,000 posterior samples are generated after 20,000 burn-ins for each sample path.

4.2 Results

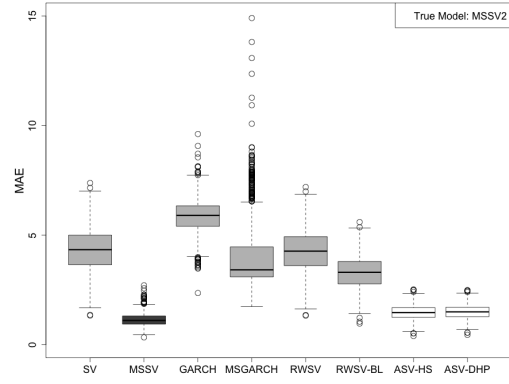
As shown in Figure 2, the SV, MSSV2, GARCH, and MSGARCH2 models achieve the lowest average MAE in DGSs 1, 2, 4, and 5, respectively, as they are the perfectly specified models for those scenarios. Both RWSV and RWSV-BL generally show similar or slightly lower accuracy compared to SV, with RWSV-BL offering only marginal improvements in DGSs 2, 3, 5, and 6, where volatility paths exhibit abrupt changes. Despite its design for trend filtering, Bayesian LASSO does not provide a significant advantage in estimating time-varying volatility compared to its counterpart with a non-informative Inverse Gamma prior, underscoring the limitations of RWSV-BL.

The proposed ASV-HS and ASV-DHS models outperform or match the true models when large volatility shifts are present, as seen in DGSs 2, 3, 5, and 6. Their accuracy is only marginally lower than that of MSSV2 in DGS 2, and slightly higher than that of MSGARCH2 in DGS 5, which are the perfectly specified models for these cases. Additionally, ASV models significantly outperform all other models in DGSs 3 and 6, showcasing their strength in capturing volatility paths with abrupt changes. However, they are less effective in stationary volatility scenarios, such as in DGSs 1 and 4, likely due to the non-mean-reverting nature of the ASV model.

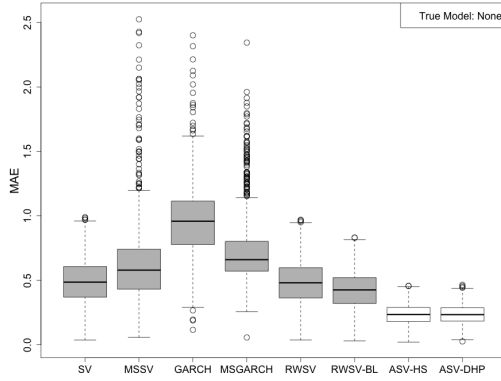
The simulation results further suggest that both Markov Switching models, MSSV2 and MSGARCH2, are less reliable than the ASV models. While they perform better on average in DGSs 1 and 4, their accuracy becomes highly variable when the assumed two-regime structure does not match the true underlying volatility process. For instance, if there is only one regime in the data, these models may produce inaccurate estimates by assigning non-zero probability to a non-existent second regime. This assumption occasionally leads to widely inconsistent estimating, resulting in high MAEs. In contrast, the ASV, which



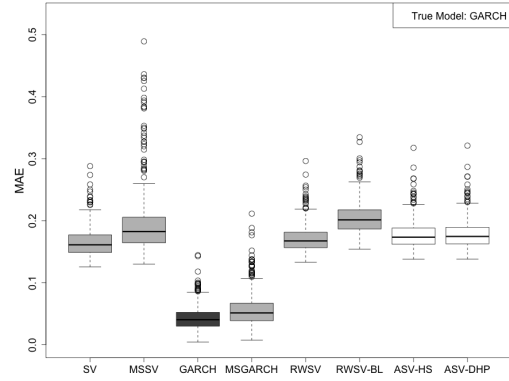
(a) DGS 1



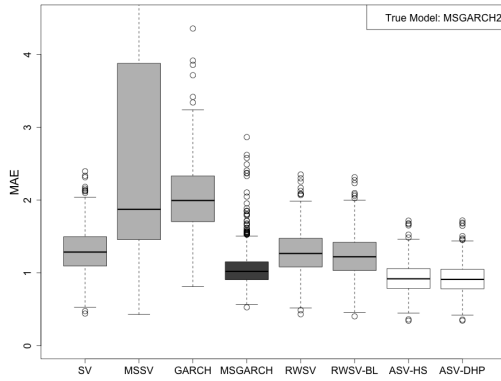
(b) DGS 2



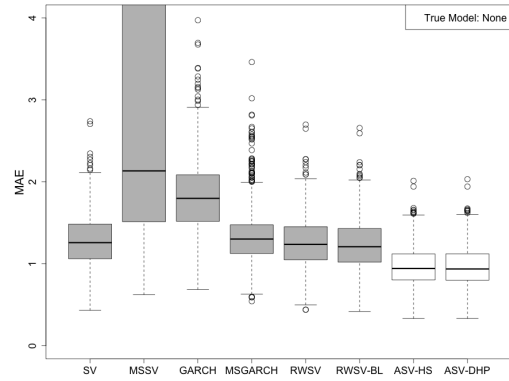
(c) DGS 3



(d) DGS 4



(e) DGS 5



(f) DGS 6

Figure 2: Box plots of Mean Absolute Error (MAE) across 1,000 sample paths comparing Stochastic Volatility (SV), Markov-Switching Stochastic Volatility with 2 Regimes (MSSV2), Generalized AutoRegressive Conditional Heteroskedasticity (GARCH), Markov-Switching GARCH with 2 regimes (MSGARCH2), Random Walk Stochastic Volatility with Inverse Gamma Prior (RWSV), Random Walk Stochastic Volatility with Bayesian LASSO (RWSV-BL), Adaptive Stochastic Volatility with Dynamic Horseshoe Prior (ASV-HS), and ASV with Dynamic Horseshoe Prior (ASV-DHP). Perfectly specified models, drawn in black, are SV and MSSV2 for DGS 1 and 2 and GARCH and MSGARCH2 for DGS 4 and 5, respectively. All models are misspecified for DGS 3 and 6.

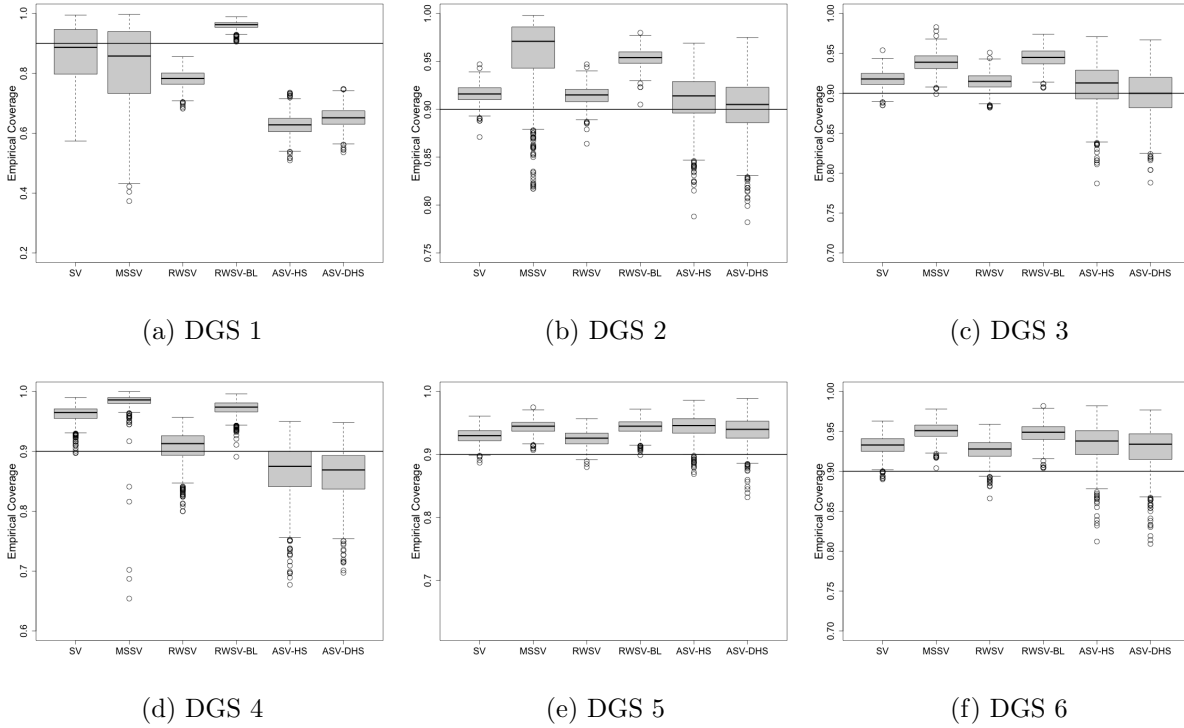


Figure 3: Box plots of empirical coverage of the 90% credible region across 1,000 sample paths of Bayesian methods: Stochastic Volatility (SV), Markov-Switching Stochastic Volatility with 2 Regimes (MSSV2), Random Walk Stochastic Volatility with Inverse Gamma Prior (RWSV), Random Walk Stochastic Volatility with Bayesian LASSO (RWSV-BL), Adaptive Stochastic Volatility with Dynamic Horseshoe Prior (ASV-HS), and ASV with Dynamic Horseshoe Prior (ASV-DHS). The horizontal line is drawn at the 90%.

does not rely on a fixed regime structure, offers greater flexibility and more consistent performance across various volatility scenarios.

Figure 3 presents the empirical coverage of the 90% credible intervals for the six Bayesian methods in the simulation study: SV, MSSV2, RWSV, RWSV-BL, ASV-HS, and ASV-DHS. The existing models—SV, MSSV2, RWSV, and RWSV-BL—generally maintain reasonable nominal coverage across all DGSs. The proposed models, ASV-HS and ASV-DHS, also achieve correct nominal coverage (90%) in DGSs 2, 3, 5, and 6. However, they significantly underperform in DGS 1 and slightly underperform in DGS 4, likely due to their assumption of nonstationarity, which conflicts with the stationary volatility paths in those two cases.

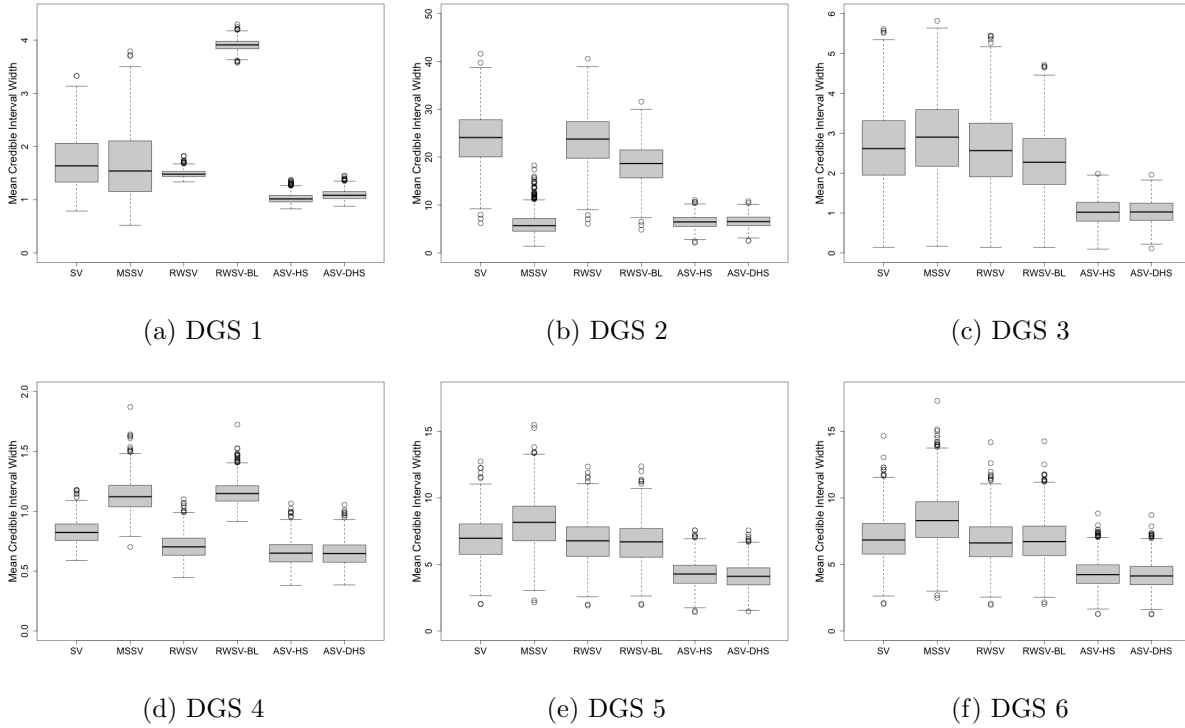


Figure 4: Box plots of mean credible interval widths (MCIW) of the 90% credible region across 1,000 sample paths of Bayesian methods: Stochastic Volatility (SV), Markov-Switching Stochastic Volatility (MSSV2), Random Walk Stochastic Volatility with Inverse Gamma Prior (RWSV), Random Walk Stochastic Volatility with Bayesian LASSO (RWSV-BL), Adaptive Stochastic Volatility with Dynamic Horseshoe Prior (ASV-HS), and ASV with Dynamic Horseshoe Prior(ASV-DHS).

Figure 4 illustrates the width of the 90% credible intervals, showing that the proposed models have the narrowest credible intervals across all DGSs. Maintaining a narrow credible interval while still achieving the correct coverage is a significant advantage, as it indicates both precise estimates and robust uncertainty quantification. In this respect, the proposed models outperform the existing ones in DGSs 2, 3, 5, and 6.

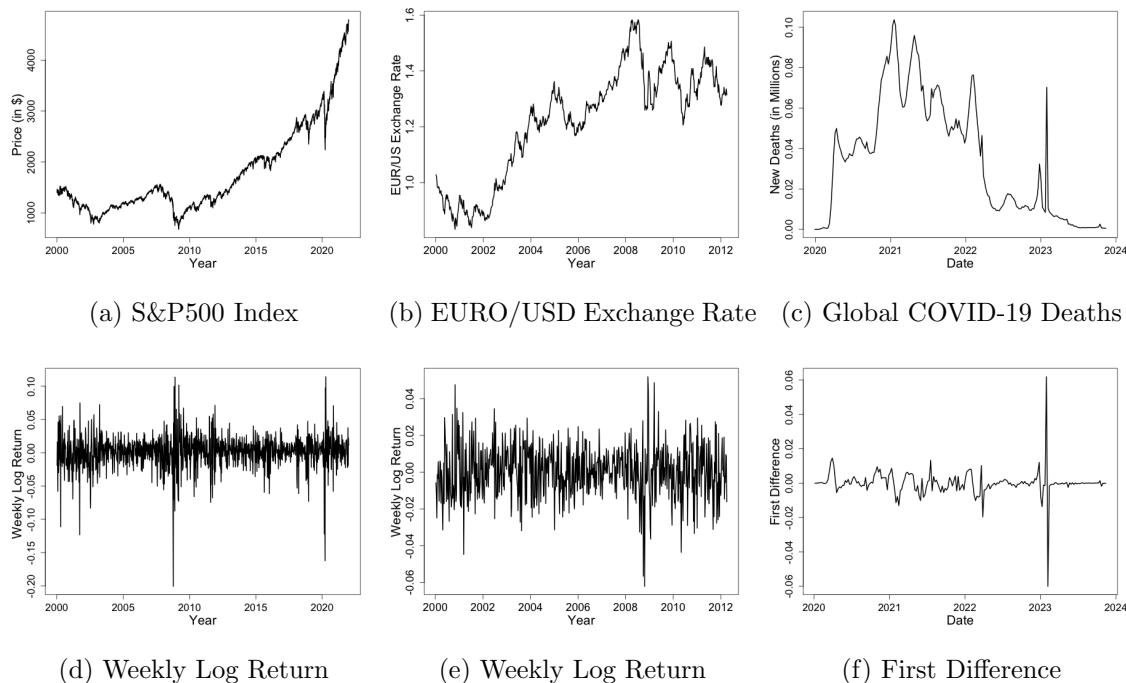


Figure 5: Price of S&P500 between 2012-01-01 and 2021-12-31 (a), EURO/USD exchange rate between 2000-01-03 and 2012-04-04 (b) and weekly COVID-19 new death tolls between 2020-01-03 to 2023-11-13 (c) in the United States are drawn. The weekly log return series for S&P500 and the exchange rate series are drawn in (d) and (e). The first difference series of COVID-19 death tolls are drawn in (f).

5 Empirical Study

5.1 Set-up

We apply ASV-DHS to empirical datasets and compare its volatility estimates with those from Stochastic Volatility (SV) and Random Walk Stochastic Volatility (RWSV) models. Specifically, we analyze the price of S&P500 from 2012-01-01 to 2021-12-31 ($n = 1148$, Figure 5a), EURO to US Dollar exchange rate between 2000-01-03 to 2012-04-04 ($n = 639$, Figure 5b), and new deaths from COVID-19 from 2020-01-03 to 2023-11-13 ($n = 202$, Figure 5c). ASV model is applied to the weekly log return series for S&P 500 and EURO/USD exchange (Figure 5d and Figure 5e), and the weekly first difference series for

COVID-19 death tolls in the U.S. (Figure 5f).

5.2 Results

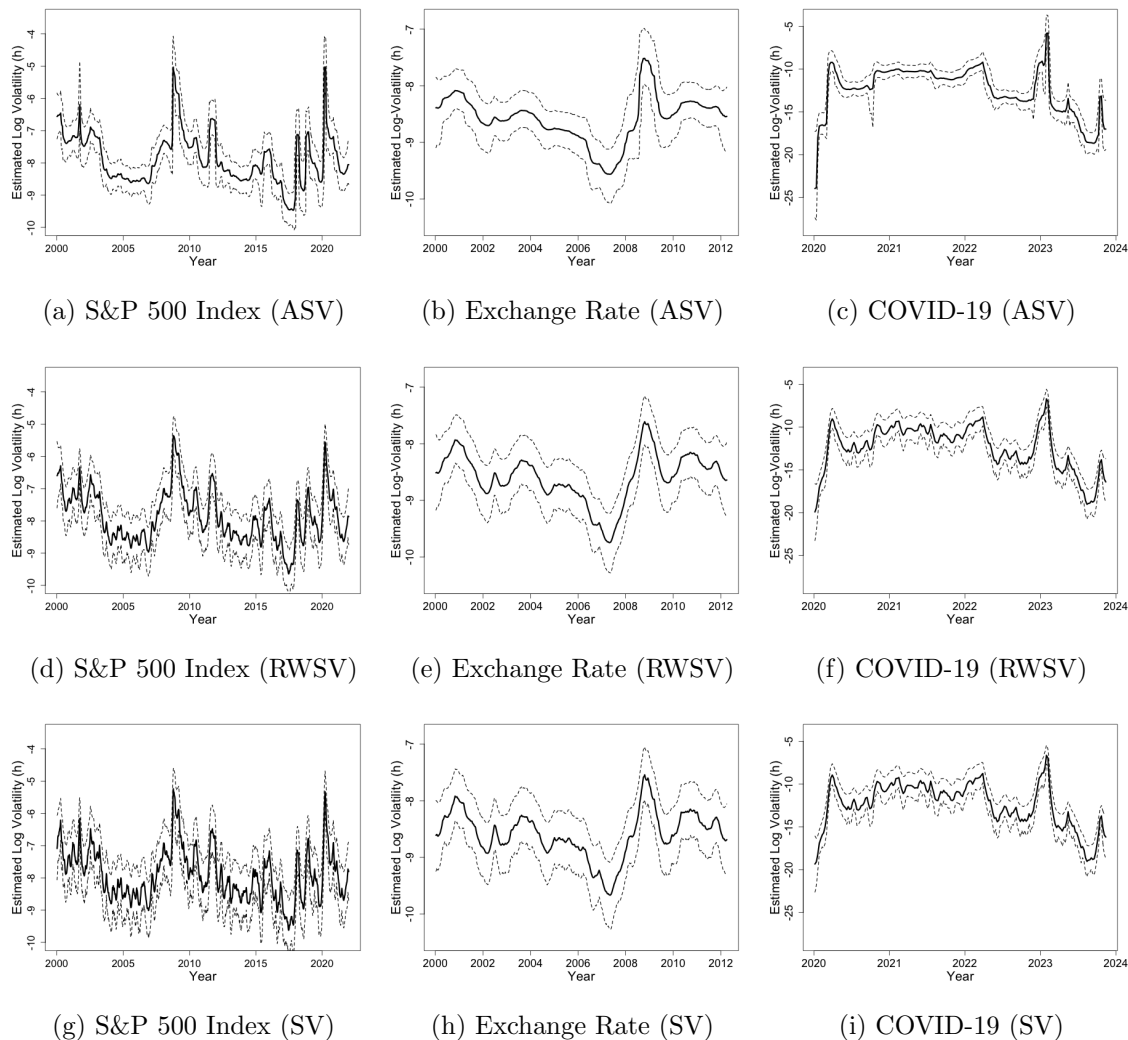


Figure 6: Estimated h with 90% quantile-based credible regions on weekly returns on S&P 500 between 2000-01-01 and 2021-12-31, weekly returns on EURO/USD exchange rate between 2000-01-03 and 2012-04-04, and weekly changes in COVID-19 death tolls in the U.S. between 2020-01-03 and 2023-11-13 based on Adaptive Shrinkage Process with Dynamic Shrinkage Process (ASV-DHS) shown in (a),(b), and (c), based on Random Walk Stochastic Volatility with inverse Gamma prior (RWSV) shown in (d), (e), and (f) and based on Stochastic Volatility (SV) model shown in (g),(h), and (i).

We assess log-volatility estimates (h_t) from ASV-DHS, RWSV, and SV across three datasets (Figure 6). For the S&P 500 dataset (Figures 6a, 6d and 6g), major volatility

spikes are observed in 2009 and 2020, corresponding to the financial crisis and COVID-19. Moderate changes appear around 2001 (9/11) and 2011 (European Debt crisis), with significant volatility in 2018 due to government shutdowns. While ASV captures these shifts well, SV and RWSV show more noise, obscuring smaller volatility changes. For the EURO/USD exchange rate (Figures 6b, 6e and 6h), there is a clear, steady volatility decline from 2001 to 2008, followed by a spike in 2008–2009 (financial crisis) and a minor increase in 2010–2011 (European Debt crisis). ASV captures this pattern smoothly, making it easier to observe the declining volatility trend compared to the noisier outputs of SV and RWSV. In COVID-19 death tolls, all models detect a sharp volatility spike at the pandemic’s onset in early 2020 and again in early 2023 (Figures 6c, 6f and 6i). Seasonal effects are evident, with increased volatility at year-ends and decreases during summer, particularly in 2022 and 2023. This seasonal pattern is clearer in ASV estimates than in SV and RWSV, where it is less discernible.

Across all datasets, ASV produces smoother volatility estimates than SV and RWSV, enhancing interpretability. This smoother output allows ASV-DHS to better capture small-to-medium volatility changes, distinguishing signal from noise more effectively than the noisier SV and RWSV estimates. Consequently, ASV provides a clearer view of underlying patterns and trends.

Another distinguishing feature of ASV is its locally adaptive credible region. Due to time-varying variance term $\tau\lambda_t = \exp\{v_t/2\}$, credible region around h_t produced by ASV-DHS also changes over time. The mean-centered credible regions generated by SV, RWSV and ASV on the three data sets are illustrated in Figure 7. Notably, the credible regions maintain a constant width for both SV and RWSV model across the sample path with RWSV having slightly narrower credible region. The credible region around h for ASV,

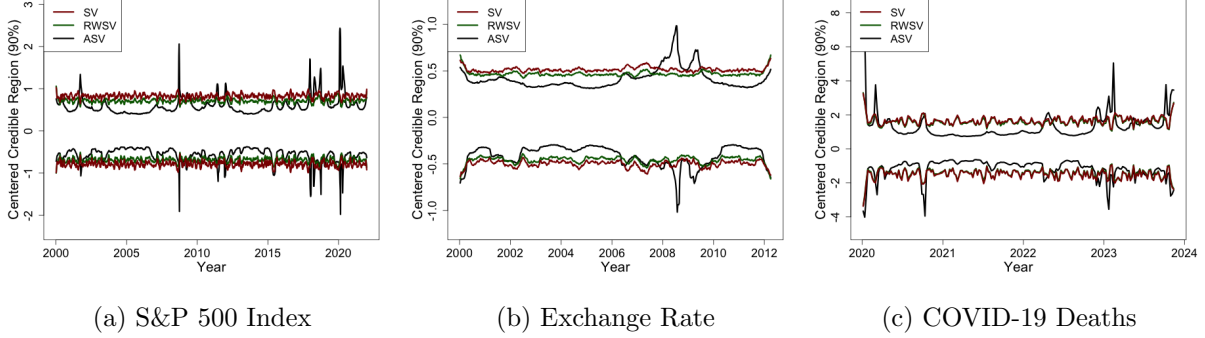


Figure 7: The 90% quantile-based credible regions on the log-variance h_t are subtracted by its posterior sample mean. The three datasets include weekly returns on S&P 500 between 2000-01-01 and 2021-12-31, weekly returns on EURO/USD exchange rate between 2000-01-03 and 2012-04-04, and weekly changes in COVID-19 death tolls between 2020-01-03 and 2023-11-13 in the U.S. The centered credible regions for Adaptive Stochastic Volatility with Dynamic Shrinkage Processes (ASV-DHS) are drawn in black, the ones based on Stochastic Volatility (SV) model are in dark red and the ones based on Random Walk Stochastic Volatility (RWSV) model are in dark green.

on the other hand, exhibits local adaptability. Specifically, the patterns on the centered credible regions match that of h_t explored in previous paragraphs. When changes in h_t are slow moving, the width of the credible region is narrow; while abrupt changes in h_t induce large credible regions.

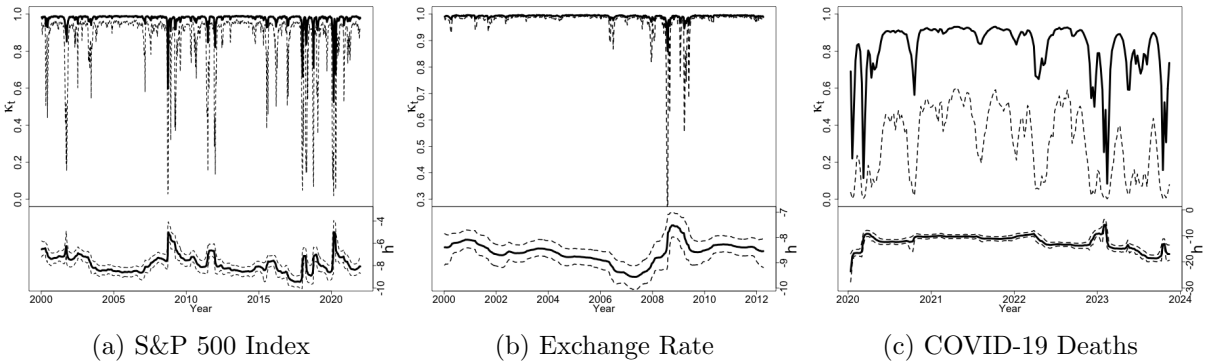


Figure 8: Comparison between the expected shrinkage parameter $\kappa_t := \frac{1}{1+\text{var}(\omega_t|\tau, \lambda_t)} = \frac{1}{1+\exp\{v_t\}} = \frac{1}{1+\tau^2\lambda_t^2}$ and expected h_t based on Adaptive Stochastic Volatility with Dynamic Horseshoe Prior (ASV-DHS) estimated on weekly returns on S&P 500 between 2000-01-01 and 2021-12-31, weekly returns on EURO/USD exchange rate between 2000-01-03 and 2012-04-04, and weekly changes in COVID-19 death tolls in the U.S. between 2020-01-03 and 2023-11-13, respectively. The dotted lines represent the one-sided 95th and centered 90th percentile credible regions for κ_t and h_t respectively.

Lastly, we analyze the empirical shrinkage parameter κ_t . The parameter v_t represents the log-variance term of Δh_t . A small v_t corresponds to minor changes in h_t , while a large v_t signifies substantial variations. Alternatively, v_t can be seen as influencing the degree of shrinkage applied to h_t , denoted as $\kappa_t := \frac{1}{1+\text{var}(\omega_t|\tau,\lambda_t)} = \frac{1}{1+\exp(v_t)} = \frac{1}{1+\tau^2\lambda_t^2}$. Analyzing κ_t rather than v_t is preferred for clarity since $\kappa_t \in (0, 1)$, unlike $v_t \in (-\infty, +\infty)$. A high κ_t (near 1) indicates strong model certainty, while a low κ_t (near 0) indicates less certainty in the estimate. Figure 8 shows the comparison between the estimated log-volatility h_t and the shrinkage parameter κ_t . As expected in ASV, prominent peaks in h_t correspond to κ_t values near 0. During periods of gradual evolution, κ_t is close to 1. Generally, κ_t for the COVID-19 deaths data is more volatile than for the S&P 500 and exchange rate data, indicating lower certainty in the model's estimates. This could be due to the smaller sample size of the COVID-19 dataset (203 data points) compared to the S&P 500 (1148 data points) and exchange rate (639 data points) datasets.

6 Trend Filtering Jointly in Mean and Variance

The Bayesian Trend Filter with the Dynamic Shrinkage processes (BTF-DSP) by Kowal et al. [2019] provides a smooth and locally adaptive estimate of the mean of a time series. We propose an extension called BTF-ASV by incorporating ASV on the error process of BTF, thereby allowing locally adaptive estimates of both the mean process β_t and the log variance process h_t simultaneously. Exact specification of the model is discussed in Model 1. In this section, we apply this method to analyze monthly global land surface air temperature anomaly with reference period 1951-1980 in 0.01 degree Celsius from 1880 to 2018. The data maybe found in this url: https://data.giss.nasa.gov/gistemp/tabledata_v3/GLB.Ts.txt.

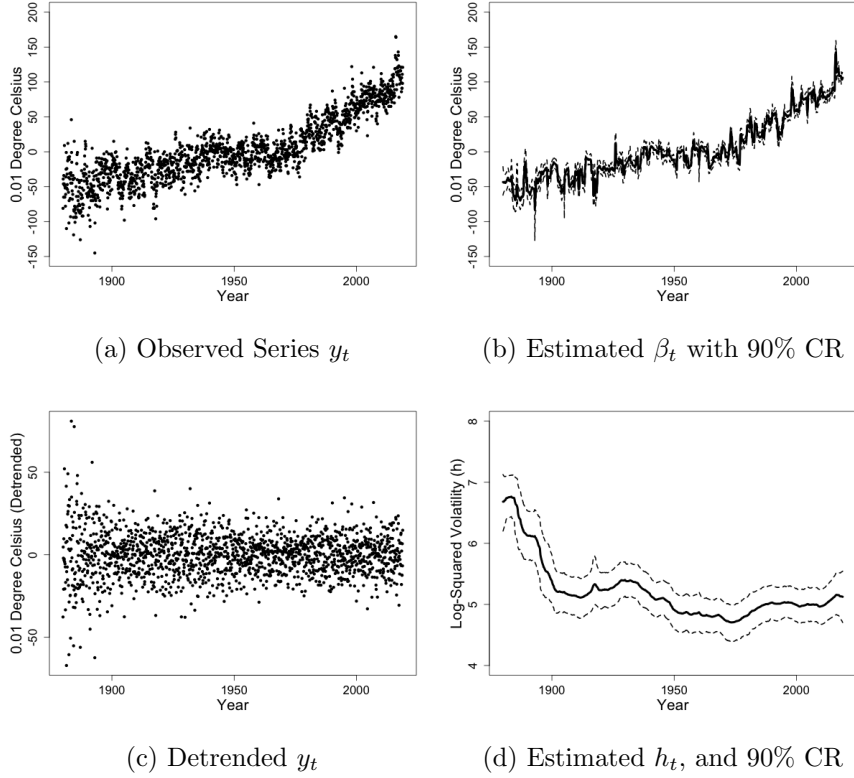


Figure 9: The monthly average global land surface air temperature anomaly from 1880 to 2018 with average temperature between 1950 and 1980 as base is illustrated in figure (a). Bayesian Trend Filter with Adaptive Stochastic Volatility is used to estimate the mean trend β_t and is illustrated in (b) with 90% credible region. Posterior mean for β_t was subtracted from the observed series to detrend the series and are illustrated in (c). BTF-ASV estimate of log-variance, h_t and its 90% credible regions is shown in (d).

The global temperature has demonstrated a consistent upward trend from 1880 to 2018 (Figure 6). This is reflected in the estimated posterior mean for β , showing a similar but smoother pattern. It is important to note that despite the model’s tendency to generate a smooth estimate, local trends still persist. This is likely attributed to yearly seasonal fluctuations as well large scale climate pattern such as El Niño and La Niña. Furthermore, there is a discernible shift in volatility over time. Notably, before 1900, extreme temperatures occurred more frequently, with wider range of fluctuations in temperature. Post-1900, however, temperatures remained within a narrower range, with occasional outliers. This pattern is captured by our estimation of log variance. The calculated volatility

peaks around 1880 and gradually decreases until 1900. Subsequently, between 1900 and 2018, volatility appears to stabilize, as illustrated in Figure 6.

7 Conclusion

In this paper, we extend the RWSV model to create a flexible and adaptive framework for modeling time-varying volatility with both abrupt and gradual changes. Initially, we introduce RWSV-BL, incorporating the time-varying variance of Δh_t with a popular shrinkage prior, Bayesian LASSO. However, our simulation study reveals that RWSV-BL is sub-optimal compared to existing models; we enhance RWSV-BL by applying a global-local shrinkage prior to the variance of Δh_t , leading to the development of ASV.

Using the global-local shrinkage prior introduced by Kowal et al. [2019], we develop two versions: ASV-HS and ASV-DHS. Extensive simulation studies show ASV demonstrates high accuracy, producing narrower credible intervals than the existing models while maintaining correct coverage, especially when the true volatility path exhibits large changes. Unlike Markov-Switching models, ASV does not require specifying the number of regimes and exhibits lower misspecification error. However, its performance declines when the volatility path is mean-reverting. ASV's ability to produce smooth yet locally adaptive estimates is also a big advantage as it offers more interpretable results.

Finally, we integrate ASV into the error process of the Bayesian Trend Filter proposed in Kowal et al. [2019], resulting in BTF-ASV. Empirical studies reveal its ability to produce smooth estimates of both time-varying mean and time-varying variance. Future research directions could explore the applications of ASV and DSP-ASV in diverse fields such as Finance, Environmental Science, and Epidemiology, leveraging their adaptability in modeling time-series exhibiting complex patterns.

8 Acknowledgement

Financial support from National Science Foundation grants OAC-1940124 and DMS-2114143 is gratefully acknowledged.

9 Supplementary Material

Appendices: A document including detailed proofs on the properties of Dynamic Shrinkage Processes (DSP) in section A. The exact prior distributions and detailed derivations of the full conditional distributions for Gibbs sampling in section.

References

- Jorge Achcar, Ricardo de Oliveira, and Emerson Barili. Use of stochastic volatility models in epidemiological data: Application to a dengue time series in são paulo city, brazil. *Journal of Biostatistics and Epidemiology*, 6(1):19–29, Oct. 2020. doi: 10.18502/jbe.v6i1.4755. URL <https://jbe.tums.ac.ir/index.php/jbe/article/view/338>.
- David Ardia, Keven Bluteau, Kris Boudt, and Leopoldo Catania. Forecasting risk with markov-switching garch models: A large-scale performance study. *International Journal of Forecasting*, 34(4):733–747, 2018.
- David Ardia, Keven Bluteau, Kris Boudt, Leopoldo Catania, and Denis-Alexandre Trottier. Markov-switching garch models in r: The msgarch package. *Journal of Statistical Software*, 91(4):1–38, 2019. doi: 10.18637/jss.v091.i04.
- Taylor B. Arnold and Ryan J. Tibshirani. *genlasso: Path Algorithm for Generalized Lasso Problems*, 2022. URL <https://CRAN.R-project.org/package=genlasso>. R package version 1.6.1.
- O. Barndorff-Nielsen, J. Kent, and M. Sørensen. Normal variance-mean mixtures and z distributions. *International Statistical Review / Revue Internationale de Statistique*, 50(2):145–159, 1982. ISSN 03067734, 17515823. URL <http://www.jstor.org/stable/1402598>.
- Luc Bauwens, Arie Preminger, and Jeroen V. K. Rombouts. Theory and inference for a markov switching garch model. *The Econometrics Journal*, 13(2):218–244, 2010. ISSN 13684221, 1368423X. URL <http://www.jstor.org/stable/23117467>.

- Anindya Bhadra, Jyotishka Datta, Nicholas G. Polson, and Brandon Willard. The horse-shoe+ estimator of ultra-sparse signals, 2015.
- Monica Billio, Roberto Casarin, and Anthony Osuntuyi. Efficient gibbs sampling for markov switching garch models. *Computational Statistics & Data Analysis*, 100:37–57, 2016. ISSN 0167-9473. doi: <https://doi.org/10.1016/j.csda.2014.04.011>. URL <https://www.sciencedirect.com/science/article/pii/S0167947314001182>.
- Tim Bollerslev. Generalized autoregressive conditional heteroskedasticity. *Journal of Econometrics*, 31(3):307–327, 1986. ISSN 0304-4076. doi: [https://doi.org/10.1016/0304-4076\(86\)90063-1](https://doi.org/10.1016/0304-4076(86)90063-1). URL <https://www.sciencedirect.com/science/article/pii/0304407686900631>.
- Celso Brunetti, Chiara Scotti, Roberto S Mariano, and Augustine HH Tan. Markov switching garch models of currency turmoil in southeast asia. *Emerging Markets Review*, 9(2): 104–128, 2008.
- Annalisa Cadonna, Sylvia Frühwirth-Schnatter, and Peter Knaus. Triple the gamma – a unifying shrinkage prior for variance and variable selection in sparse state space and tvp models, 2019.
- Jun Cai. A markov model of switching-regime arch. *Journal of Business & Economic Statistics*, 12(3):309–316, 1994. ISSN 07350015. URL <http://www.jstor.org/stable/1392087>.
- CARLOS M. Carvalho, NICHOLAS G. POLSON, and JAMES G. SCOTT. The horseshoe estimator for sparse signals. *Biometrika*, 97(2):465–480, 2010. ISSN 00063444, 14643510. URL <http://www.jstor.org/stable/25734098>.
- Ray Yeutien Chou. Volatility persistence and stock valuations: Some empirical evidence using garch. *Journal of Applied Econometrics*, 3(4):279–294, 1988. ISSN 08837252, 10991255. URL <http://www.jstor.org/stable/2096644>.
- Robert F. Engle. Autoregressive conditional heteroscedasticity with estimates of the variance of united kingdom inflation. *Econometrica*, 50(4):987–1007, 1982. ISSN 00129682, 14680262. URL <http://www.jstor.org/stable/1912773>.
- Kenneth French, G. Schwert, and Robert Stambaugh. Expected stock returns and volatility. *Journal of Financial Economics*, 19(1):3–29, 1987. URL <https://EconPapers.repec.org/RePEc:eee:jfinec:v:19:y:1987:i:1:p:3-29>.
- Stephen F. Gray. Modeling the conditional distribution of interest rates as a regime-switching process. *Journal of Financial Economics*, 42(1):27–62, September 1996a. URL <https://ideas.repec.org/a/eee/jfinec/v42y1996i1p27-62.html>.
- Stephen F. Gray. Modeling the conditional distribution of interest rates as a regime-switching process. *Journal of Financial Economics*, 42(1):27–62, 1996b. ISSN 0304-405X. doi: [https://doi.org/10.1016/0304-405X\(96\)00875-6](https://doi.org/10.1016/0304-405X(96)00875-6). URL <https://www.sciencedirect.com/science/article/pii/0304405X96008756>.

- James D. Hamilton. A new approach to the economic analysis of nonstationary time series and the business cycle. *Econometrica*, 57(2):357–384, 1989. ISSN 00129682, 14680262. URL <http://www.jstor.org/stable/1912559>.
- James D Hamilton and Raul Susmel. Autoregressive conditional heteroskedasticity and changes in regime. *Journal of Econometrics*, 64(1):307–333, 1994. ISSN 0304-4076. doi: [https://doi.org/10.1016/0304-4076\(94\)90067-1](https://doi.org/10.1016/0304-4076(94)90067-1). URL <https://www.sciencedirect.com/science/article/pii/0304407694900671>.
- Andrew Harvey, Esther Ruiz, and Neil Shephard. Multivariate stochastic variance models. *The Review of Economic Studies*, 61(2):247–264, 04 1994. ISSN 0034-6527. doi: 10.2307/2297980. URL <https://doi.org/10.2307/2297980>.
- JOHN Hull and ALAN White. The pricing of options on assets with stochastic volatilities. *The Journal of Finance*, 42(2):281–300, 1987. doi: <https://doi.org/10.1111/j.1540-6261.1987.tb02568.x>. URL <https://onlinelibrary.wiley.com/doi/abs/10.1111/j.1540-6261.1987.tb02568.x>.
- Soosung Hwang, Steve E. Satchell, and Pedro L. Valls Pereira. How Persistent is Volatility? An Answer with Stochastic Volatility Models with Markov Regime Switching State Equations. Econometric Society 2004 Latin American Meetings 198, Econometric Society, August 2004. URL <https://ideas.repec.org/p/ecm/latm04/198.html>.
- Eric Jacquier, Nicholas G. Polson, and Peter E. Rossi. Bayesian analysis of stochastic volatility models. *Journal of Business & Economic Statistics*, 12(4):371–389, 1994. ISSN 07350015. URL <http://www.jstor.org/stable/1392199>.
- Gregor Kastner. Dealing with stochastic volatility in time series using the R package stochvol. *Journal of Statistical Software*, 69(5):1–30, 2016. doi: 10.18637/jss.v069.i05.
- Gregor Kastner and Sylvia Frühwirth-Schnatter. Ancillarity-sufficiency interweaving strategy (ASIS) for boosting MCMC estimation of stochastic volatility models. *Computational Statistics & Data Analysis*, 76:408–423, aug 2014. doi: 10.1016/j.csda.2013.01.002. URL <https://doi.org/10.1016%2Fj.csda.2013.01.002>.
- Sangjoon Kim, Neil Shephard, and Siddhartha Chib. Stochastic volatility: Likelihood inference and comparison with arch models. *The Review of Economic Studies*, 65(3):361–393, 1998. ISSN 00346527, 1467937X. URL <http://www.jstor.org/stable/2566931>.
- Seung-Jean Kim, Kwangmoo Koh, Stephen Boyd, and Dimitry Gorinevsky. l_1 trend filtering. *SIAM Rev.*, 51(2):339–360, 2009. ISSN 0036-1445,1095-7200. doi: 10.1137/070690274. URL <https://doi.org/10.1137/070690274>.
- Polychronis Kostoulas, Eletherios Meletis, Konstantinos Pateras, Paolo Eusebi, Theodoros Kostoulas, Luis Furuya-Kanamori, Niko Speybroeck, Matthew Denwood, Suhail Doi, Christian Althaus, Carsten Kirkeby, Pejman Rohani, Navneet Dhand, José Peñalvo, Lehana Thabane, Ben miled Slimane, Hamid Sharifi, and Stephen Walter. The epidemic volatility index, a novel early warning tool for identifying new waves in an epidemic. *Scientific Reports*, 11:23775, 12 2021. doi: 10.1038/s41598-021-02622-3.

- Daniel R. Kowal, David S. Matteson, and David Ruppert. Dynamic Shrinkage Processes. *Journal of the Royal Statistical Society Series B: Statistical Methodology*, 81(4):781–804, 05 2019. ISSN 1369-7412. doi: 10.1111/rssb.12325. URL <https://doi.org/10.1111/rssb.12325>.
- Jiaxin Ma, Feiyun Xu, Kai Huang, and Ren Huang. Gnar-garch model and its application in feature extraction for rolling bearing fault diagnosis. *Mechanical Systems and Signal Processing*, 93:175–203, 2017.
- Saeid Mehdizadeh, Javad Behmanesh, and Keivan Khalili. A comparison of monthly precipitation point estimates at 6 locations in iran using integration of soft computing methods and garch time series model. *Journal of Hydrology*, 554:721–742, 2017. ISSN 0022-1694. doi: <https://doi.org/10.1016/j.jhydrol.2017.09.056>. URL <https://www.sciencedirect.com/science/article/pii/S0022169417306601>.
- Angelo Melino and Stuart M. Turnbull. Pricing foreign currency options with stochastic volatility. *Journal of Econometrics*, 45(1-2):239–265, 1990. URL <https://EconPapers.repec.org/RePEc:eee:econom:v:45:y:1990:i:1-2:p:239-265>.
- Reza Modarres and Taha BMJ Ouarda. Modeling the relationship between climate oscillations and drought by a multivariate garch model. *Water Resources Research*, 50(1):601–618, 2014.
- Haruhisa Nishino and Kazuhiko Kakamu. A random walk stochastic volatility model for income inequality. *Japan and the World Economy*, 36:21–28, 2015. ISSN 0922-1425. doi: <https://doi.org/10.1016/j.japwor.2015.06.003>. URL <https://www.sciencedirect.com/science/article/pii/S0922142515000328>.
- Yasuhiro Omori, Siddhartha Chib, Neil Shephard, and Jouchi Nakajima. Stochastic volatility with leverage: Fast and efficient likelihood inference. *Journal of Econometrics*, 140(2):425–449, 2007. ISSN 0304-4076. doi: <https://doi.org/10.1016/j.jeconom.2006.07.008>. URL <https://www.sciencedirect.com/science/article/pii/S0304407606001436>.
- Martins Otache. Conditional heteroscedasticity in streamflow process: Paradox or reality? *Open Journal of Modern Hydrology*, 02:79–90, 01 2012. doi: 10.4236/ojmh.2012.24010.
- Trevor Park and George Casella. The bayesian lasso. *Journal of the American Statistical Association*, 103(482):681–686, 2008. doi: 10.1198/016214508000000337. URL <https://doi.org/10.1198/016214508000000337>.
- Hong Thom Pham and Bo-Suk Yang. Estimation and forecasting of machine health condition using arma/garch model. *Mechanical systems and signal processing*, 24(2):546–558, 2010.
- Nicholas G. Polson, James G. Scott, and Jesse Windle. Bayesian inference for logistic models using poly-gamma latent variables, 2013.
- Ser-Huang Poon and Stephen J. Taylor. Stock returns and volatility: An empirical study of the uk stock market. *Journal of Banking & Finance*, 16(1):37–59, 1992. ISSN 0378-4266. doi: [https://doi.org/10.1016/0378-4266\(92\)90077-D](https://doi.org/10.1016/0378-4266(92)90077-D). URL [https://doi.org/10.1016/0378-4266\(92\)90077-D](https://doi.org/10.1016/0378-4266(92)90077-D).

- [//www.sciencedirect.com/science/article/pii/037842669290077D](http://www.sciencedirect.com/science/article/pii/037842669290077D). Special Issue on European Capital Markets.
- R Core Team. *R: A Language and Environment for Statistical Computing*. R Foundation for Statistical Computing, Vienna, Austria, 2013. URL <http://www.R-project.org/>.
- Esther Ruiz. Quasi-maximum likelihood estimation of stochastic volatility models. *Journal of Econometrics*, 63(1):289–306, 1994. ISSN 0304-4076. doi: [https://doi.org/10.1016/0304-4076\(93\)01569-8](https://doi.org/10.1016/0304-4076(93)01569-8). URL <https://www.sciencedirect.com/science/article/pii/0304407693015698>.
- RR Sarkar and C Chatterjee. Application of different time series models on epidemiological data-comparison and predictions for malaria prevalence. *SM J. Biom. Biostat*, 2(4):1022, 2017.
- Toryn L. J. Schafer and David S. Matteson. Locally adaptive shrinkage priors for trends and breaks in count time series. *Technometrics*, 0(ja):1–16, 2024. doi: 10.1080/00401706.2024.2407316. URL <https://doi.org/10.1080/00401706.2024.2407316>.
- Mike K. P. So, K. Lam, and W. K. Li. A stochastic volatility model with markov switching. *Journal of Business & Economic Statistics*, 16(2):244–253, 1998. ISSN 07350015. URL <http://www.jstor.org/stable/1392580>.
- Mike K.P. So, K. Lam, and W.K. Li. An Empirical Study of Volatility in Seven Southeast Asian Stock Markets Using ARV Models. *Journal of Business Finance & Accounting*, 24(2):261–276, March 1997. doi: 10.1111/1468-5957.00104. URL <https://ideas.repec.org/a/bla/jbfnac/v24y1997i2p261-276.html>.
- Fei Su and Lei Wang. Conditional volatility persistence and realized volatility asymmetry: Evidence from the chinese stock markets. *Emerging Markets Finance and Trade*, 56(14):3252–3269, 2020. doi: 10.1080/1540496X.2019.1574566. URL <https://doi.org/10.1080/1540496X.2019.1574566>.
- S.J. Taylor. *Modelling Financial Time Series*. G - Reference, Information and Interdisciplinary Subjects Series. World Scientific, 2008. ISBN 9789812770844. URL <https://books.google.com/books?id=KQ5pDQAAQBAJ>.
- Robert Tibshirani. Regression shrinkage and selection via the lasso. *Journal of the Royal Statistical Society. Series B (Methodological)*, 58(1):267–288, 1996. ISSN 00359246. URL <http://www.jstor.org/stable/2346178>.
- Ryan J. Tibshirani. Adaptive piecewise polynomial estimation via trend filtering. *The Annals of Statistics*, 42(1), February 2014. ISSN 0090-5364. doi: 10.1214/13-aos1189. URL <http://dx.doi.org/10.1214/13-AOS1189>.
- Michael K Tippett. Changing volatility of us annual tornado reports. *Geophysical Research Letters*, 41(19):6956–6961, 2014.

- Huimin Wang, Songbai Song, Gengxi Zhang, Olusola O. Ayantobo, and Tianli Guo. Stochastic volatility modeling of daily streamflow time series. *Water Resources Research*, 59(1):e2021WR031662, 2023a. doi: <https://doi.org/10.1029/2021WR031662>. URL <https://agupubs.onlinelibrary.wiley.com/doi/abs/10.1029/2021WR031662>. e2021WR031662 2021WR031662.
- Huimin Wang, Songbai Song, Gengxi Zhang, and Olusola O. Ayantoboc. Predicting daily streamflow with a novel multi-regime switching arima-ms-garch model. *Journal of Hydrology: Regional Studies*, 47:101374, 2023b. ISSN 2214-5818. doi: <https://doi.org/10.1016/j.ejrh.2023.101374>. URL <https://www.sciencedirect.com/science/article/pii/S2214581823000617>.
- W Wang, PHAJ M Van Gelder, JK Vrijling, and J Ma. Testing and modelling autoregressive conditional heteroskedasticity of streamflow processes. *Nonlinear processes in Geophysics*, 12(1):55–66, 2005.
- MIKE West. On scale mixtures of normal distributions. *Biometrika*, 74(3):646–648, 09 1987. ISSN 0006-3444. doi: [10.1093/biomet/74.3.646](https://doi.org/10.1093/biomet/74.3.646). URL <https://doi.org/10.1093/biomet/74.3.646>.
- Haoxuan Wu, Toryn L. J. Schafer, and David S. Matteson. Trend and variance adaptive bayesian changepoint analysis and local outlier scoring. *Journal of Business & Economic Statistics*, 0(0):1–12, 2024a. doi: [10.1080/07350015.2024.2362269](https://doi.org/10.1080/07350015.2024.2362269). URL <https://doi.org/10.1080/07350015.2024.2362269>.
- Haoxuan Wu, Toryn L. J. Schafer, Sean Ryan, and David S. Matteson. Drift vs shift: Decoupling trends and changepoint analysis. *Technometrics*, 0(ja):1–16, 2024b. doi: [10.1080/00401706.2024.2365730](https://doi.org/10.1080/00401706.2024.2365730). URL <https://doi.org/10.1080/00401706.2024.2365730>.
- Diethelm Wuertz, Yohan Chalabi, Tobias Setz, Martin Maechler, and Georgi N. Boshnakov. *fGarch: Rmetrics - Autoregressive Conditional Heteroskedastic Modelling*, 2023. URL <https://www.rmetrics.org>. R package version 4031.90.

A Proofs of Theorems

A.1 Theorem 1

As mentioned, proofs directly follow from Kolmogorov's three series theorem, which state the sufficient and necessary condition for almost sure convergence of infinite sum of random variables. Let $\phi \in (0, 1)$. Due to symmetry of *sech* function, we only need to prove the case when $0 < \phi < 1$, and the case where $-1 < \phi < 0$, directly follows. For the first condition, let $\epsilon > 0$, and h is some positive integer or 0.

$$\begin{aligned}
 P(|z_h| \geq \epsilon) &= 2 \int_{\epsilon}^{\infty} \frac{\exp\{x/(2\phi^h)\}}{\pi\phi^h(1 + \exp\{x/\phi^h\})} dx \\
 &= \frac{2}{\pi\phi^h} \int_{\epsilon}^{\infty} \frac{\exp\{x/(2\phi^h)\}}{1 + \exp\{x/\phi^h\}} dx && u = \exp\{x/(2\phi^h)\} \\
 &= \frac{4}{\pi} \int_{\epsilon}^{\infty} \frac{1}{1 + u^2} du && 2\phi^h du = \exp\{x/(2\phi^h)\} dx \\
 &= \frac{4}{\pi} \arctan(\exp\{x/(2\phi^h)\}) \Big|_{\epsilon}^{\infty} \\
 &= 2\left(1 - \frac{2}{\pi} \arctan(\exp\{\epsilon/(2\phi^h)\})\right) \\
 &= \frac{4}{\pi} \operatorname{arccotan}(\exp\{\epsilon/(2\phi^h)\}) \\
 &\leq \frac{4}{\pi} \operatorname{arccotan}(\exp\{h\}) && \text{if } \epsilon \leq 2h\phi^h
 \end{aligned}$$

Since $0 < \phi < 1$, $2h\phi^h$ converges to 0. Also, $2h\phi^h \geq 0$ for $h \geq 0$. For any ϵ , we have h' that satisfies $\epsilon \leq 2h\phi^h$ for $h' \leq h$. Then, fix such h' .

$$\begin{aligned}
 \int_{h'}^{\infty} \frac{4}{\pi} \operatorname{arccotan}(\exp\{h\}) dh &< \infty \\
 \sum_{h=h'}^{\infty} \frac{4}{\pi} \operatorname{arccotan}(\exp\{\epsilon/(2\phi^h)\}) &\leq \sum_{h=h'}^{\infty} \frac{4}{\pi} \operatorname{arccotan}(\exp\{h\}) < \infty
 \end{aligned}$$

Therefore,

$$\sum_{h=0}^{\infty} P(|z_h| \geq \epsilon) = \sum_{h=0}^{\infty} \frac{4}{\pi} \operatorname{arccotan}(\exp\{\epsilon/(2\phi^h)\}) < \infty$$

On the side note, we can also easily see that when $|\phi| > 1$, the sum diverges to ∞ . By Borel-Cantelli lemma, we may conclude that $\sum_{h=0}^{\infty} z_h$ diverges almost surely.

Define $y_h = z_h 1_{\{|z_h| \leq \epsilon\}}$. For the second and the third condition, we need to show that 1) $\sum_{h=0}^{\infty} E(y_h)$ converges, and 2) $\sum_{h=0}^{\infty} \operatorname{Var}(y_h)$, converges. For the second condition, it suffices to show:

$$E\left(\sum_{h=0}^{\infty} y_h\right) = \sum_{h=0}^{\infty} E(y_h) < \infty,$$

which is satisfied by showing $\sum_{h=0}^{\infty} E(|y_h|) < \infty$ (Fubini). Using Cauchy-Schwartz Inequality:

$$\begin{aligned} \sum_{h=0}^{\infty} E(|y_h|) &= \sum_{h=0}^{\infty} E(|z_h 1_{\{|z_h| \leq \epsilon\}}|) \\ &\leq \sum_{h=0}^{\infty} \sqrt{E(z_h^2) P(|z_h| \leq \epsilon)} \\ &\leq \sum_{h=0}^{\infty} \sqrt{E(z_h^2)} = \sum_{h=0}^{\infty} \sqrt{\operatorname{Var}(z_h)} = \pi \sum_{h=0}^{\infty} \phi^h = \frac{\pi}{(1-\phi)} < \infty. \end{aligned}$$

The second condition is satisfied. For the third condition, similar logic is applied. First note that:

$$\begin{aligned} \operatorname{var}\left(\sum_{h=0}^{\infty} y_h\right) &= E\left(\left(\sum_{h=0}^{\infty} y_h\right)^2\right) + E\left(\left(\sum_{h=0}^{\infty} y_h\right)^2\right) \\ &= E\left(\left(\sum_{h=0}^{\infty} y_h\right)^2\right) + \left(\sum_{h=0}^{\infty} E(y_h)\right)^2 \\ &= E\left(\left(\sum_{h=0}^{\infty} y_h\right)^2\right). \end{aligned}$$

And,

$$\begin{aligned}
\lim_{h \rightarrow \infty} E\left(\left(\sum_{n=0}^h y_n\right)^2\right) &= \lim_{n \rightarrow \infty} E\left(\sum_{h=0}^n y_h^2\right) && (\text{independence}) \\
&= \lim_{n \rightarrow \infty} \sum_{h=0}^n E(y_h^2) = \sum_{h=0}^{\infty} E(z_h^2 1_{\{|z_h| \leq \epsilon\}}) \\
&\leq \sum_{h=0}^{\infty} E(z_h^2) = \frac{\pi^2}{(1 - \phi^2)} < \infty
\end{aligned}$$

Therefore:

$$\text{var}\left(\sum_{h=0}^{\infty} y_h\right) = \sum_{h=0}^{\infty} \text{var}(y_h) < \infty$$

All three conditions are satisfied.

A.2 Theorem 2

When $\phi = 0.5$, we have the following special case for the MGF,

$$\begin{aligned}
\prod_{h=0}^{\infty} \cos\left(\frac{\pi t}{2^h}\right) &= \prod_{h=0}^{\infty} \frac{\sin\left(\frac{\pi t}{2^{h-1}}\right)}{2 \sin\left(\frac{\pi t}{2^h}\right)} = \lim_{n \rightarrow \infty} \prod_{h=0}^n \frac{\sin\left(\frac{\pi t}{2^{h-1}}\right)}{2 \sin\left(\frac{\pi t}{2^h}\right)} \\
&= \lim_{n \rightarrow \infty} \frac{\sin(2\pi t)}{2^n \sin\left(\frac{\pi t}{2^n}\right)} = \frac{\sin(2\pi t)}{2\pi t}
\end{aligned}$$

We have:

$$\prod_{h=0}^{\infty} \sec\left(\frac{\pi t}{2^h}\right) = \frac{1}{\prod_{h=0}^{\infty} \cos\left(\frac{\pi t}{2^h}\right)} = \frac{2\pi t}{\sin(2\pi t)} = \Gamma(1 - 2t)\Gamma(1 + 2t) = \beta(1 - 2t, 1 + 2t)$$

$\frac{2\pi t}{\sin(2\pi t)} = \Gamma(1 - 2t)\Gamma(1 + 2t)$ is by the reflection relation. *Logistic*(μ, s) has the the following moment generating function $\exp(-\mu t)\beta(1 - st, 1 + st)$. Since the moment generating

function uniquely determines the random variable, and by Theorem 2,

$$z_t = \sum_{h=0}^{\infty} z_{t,h} \xrightarrow{a.s} \text{Logistic}(0, 2)$$

Note that

$$f(z_t) = \frac{1}{8} \text{sech}^2\left(\frac{z_t}{4}\right)$$

A.3 Theorem 3

Let $\lambda_t := \exp(v_t)$. We showed that $f(\lambda_t) = \frac{1}{(1+\lambda_t)^2}$. We have:

$$f(\Delta h_t) = \int_0^{\infty} \frac{1}{\sqrt{2\pi\lambda_t^2}} \exp\left(-\frac{\Delta^2 h_t}{2\lambda_t^2}\right) \frac{1}{(1+\lambda_t)^2} d\lambda_t$$

$\forall x > 0$,

$$\frac{1}{2(1+x^2)} \leq \frac{1}{(1+x)^2} \leq \frac{1}{(1+x^2)}.$$

Thus,

$$\begin{aligned} f(\Delta h_t) &\leq \int_0^{\infty} \frac{1}{\sqrt{2\pi\lambda_t^2}} \exp\left(-\frac{\Delta^2 h_t}{2\lambda_t^2}\right) \frac{1}{(1+\lambda_t^2)} d\lambda_t \\ &= \frac{1}{2\sqrt{2\pi}} \int_0^{\infty} \frac{1}{1+u} \exp\left(-\frac{u\Delta^2 h_t}{2}\right) du && u = \frac{1}{\lambda_t^2} \\ &= \frac{1}{2\sqrt{2\pi}} \exp(\Delta^2 h_t/2) E_1(\Delta^2 h_t/2), \end{aligned}$$

where $E_1()$ is the exponential integral function, which satisfies the following upper and lower bound $\forall t > 0$:

$$\frac{\exp(-t)}{2} \log\left(1 + \frac{2}{t}\right) < E_1(t) < \exp(-t) \log\left(1 + \frac{1}{t}\right)$$

Thus,

$$f(\Delta h_t) < \frac{1}{2\sqrt{2\pi}} \log\left(1 + \frac{2}{\Delta^2 h_t}\right)$$

Similarly for the lower bound,

$$f(\Delta h_t) > \frac{1}{8\sqrt{2\pi}} \log\left(1 + \frac{4}{\Delta^2 h_t}\right)$$

The lower and upper bound for $\Delta h_t \neq 0$ is shown. The lower bound clearly approaches infinity as Δh_t approaches 0, which completes the proof.

B Full Conditional for Gibbs Sampling

B.1 j

$\mathbf{j} = (j_1, \dots, j_T)$ was introduced to expand the likelihood on y^* . In this section, we show that $\forall k \in \{1, \dots, 10\}$:

$$\begin{aligned} p(j_t = k | h_t, v_t, s_t, \xi_t, \mu, \xi_\mu, \phi, y_t^*) &= p(j_t = k | h_t, y_t^*) \\ &= \frac{\mathcal{N}(y_t^* | h_t + \mu_k, \sigma_k^2) p_k}{\sum_{i=1}^{10} p_i \mathcal{N}(y_t^* | h_t + \mu_i, \sigma_i^2)}, \quad \forall t \in \{1, \dots, T\} \end{aligned}$$

\mathbf{j} is only associated with y^* , which is only associated with \mathbf{h} and \mathbf{j} :

$$p(j_t = k | h_t, v_t, s_t, \xi_t, \mu, \xi_\mu, \phi, y_t^*) = p(j_t = k | h_t, y_t^*) = \frac{f(y_t^* | h_t, j_t) p(j_t = k)}{\int f(y_t^* | h_t, j_t) f(j_t) dj_t}$$

By Omori et al. [2007],

$$f(y_t^* | j_t, h_t) = \mathcal{N}(y_t^* | h_t + \mu_{j_t}, \sigma_{j_t}^2)$$

Naturally, $\forall k \in \{1, \dots, 10\}$

$$\begin{aligned} p(j_t = k | h_t, y_t^*) &= \frac{f(y_t^* | h_t, j_t = k) p(j_t = k)}{f(y_t^* | h_t)} \\ &= \frac{f(y_t^* | h_t, j_t = k) p(j_t = k)}{\sum_{i=1}^{10} p(j_t = i) f(y_t^* | h_t, j_t = i)} \\ &= \frac{\mathcal{N}(y_t^* | h_t + \mu_k, \sigma_k^2) p_k}{\sum_{i=1}^{10} p_i \mathcal{N}(y_t^* | h_t + \mu_i, \sigma_i^2)}, \quad \forall t \in \{1, \dots, T\}, \end{aligned}$$

which is what we wanted to show. Exact distribution on $j_t \stackrel{i.i.d.}{\sim} \text{Categorical}(p_1, \dots, p_{10})$ as well as corresponding mean and the variance parameter of each component is described in Omori et al. [2007].

B.2 h

The likelihood and the conditional priors on \mathbf{h} are:

$$\begin{aligned} f(y^* | \mathbf{j}, \mathbf{h}) &= \prod_{t=1}^T \mathcal{N}(y_t^* | h_t + \mu_{j_t}, \sigma_{j_t}^2) = \mathcal{N}(y^* | h + \mu_j, I\sigma_j^2) \\ f(\mathbf{h} | \mathbf{v}) &= \mathcal{N}(h_1 | 0, e^{v_1}) \prod_{t=1}^T \mathcal{N}(h_t | h_{t-1}, e^{v_t}) \end{aligned}$$

Note that \mathbf{h} , a conditionally Gaussian, is a linear combination of $\Delta\mathbf{h}$, Specifically, $\mathbf{h} = A_h\Delta\mathbf{h}$ with

$$A_h := \begin{bmatrix} 1 & & & & 0 \\ & 1 & & & \\ & 1 & 1 & & \\ & \vdots & \vdots & \ddots & \ddots \\ & 1 & 1 & \dots & \dots & 1 \end{bmatrix}$$

Thus, the precision of the conditional prior of h is a tridiagonal matrix Q_v

$$Q_v := \begin{bmatrix} \left(\frac{1}{e^{v_2}} + \frac{1}{e^{v_1}}\right) & -\frac{1}{e^{v_2}} & 0 & \dots & \dots & 0 \\ -\frac{1}{e^{v_2}} & \left(\frac{1}{e^{v_3}} + \frac{1}{e^{v_2}}\right) & -\frac{1}{e^{v_3}} & \ddots & \ddots & \vdots \\ 0 & -\frac{1}{e^{v_3}} & \left(\frac{1}{e^{v_4}} + \frac{1}{e^{v_3}}\right) & -\frac{1}{e^{v_4}} & \ddots & \ddots \\ \vdots & \ddots & \ddots & \ddots & \ddots & 0 \\ \vdots & \ddots & \ddots & -\frac{1}{e^{v_{T-1}}} & \left(\frac{1}{e^{v_{T-1}}} + \frac{1}{e^{v_T}}\right) & -\frac{1}{e^{v_T}} \\ 0 & \dots & \dots & 0 & -\frac{1}{e^{v_T}} & \frac{1}{e^{v_T}} \end{bmatrix}$$

We have $f(\mathbf{h}|\mathbf{v}) = \mathcal{N}(\mathbf{h}|0, Q_v^{-1})$. Thus, we may conclude that.

$$f(\mathbf{h}|\mathbf{j}, \mathbf{v}, y^*) \propto \mathcal{N}(y^* - \mu_j | \mathbf{h}, I\sigma_j^2)\mathcal{N}(\mathbf{h}|0, Q_v^{-1}).$$

Since both the likelihood and the prior are Gaussian, the conditional posterior is also Gaussian:

$$f(\mathbf{h}|\mathbf{j}, \mathbf{v}, y^*) = \mathcal{N}\left(\mathbf{h} \left| \left(Q_v + I\frac{1}{\sigma_j^2}\right)^{-1} \frac{y - \mu_j}{\sigma_j^2}, \left(Q_v + I\frac{1}{\sigma_j^2}\right)^{-1}\right.\right).$$

B.3 v

We use the all-without-loop (AWOL) sampler by Kastner and Frühwirth-Schnatter [2014] with parameter expansion on the error term with scale mixture normal distribution for sampling \mathbf{v}, μ and ϕ . By the conditional independence, the likelihood with respect to \mathbf{v} , reduces to $f(\boldsymbol{\omega}^*|v)$ where $\omega_1^* = \log(h_1^2)$ and $\omega_t^* = \log((h_t - h_{t-1})^2), \forall t \geq 2$. With the parameter expansion on the likelihood with 10-component Gaussian Mixture proposed by Omori et al. [2007],

$$f(\boldsymbol{\omega}^*|\mathbf{v}, \mathbf{s}) = \mathcal{N}(\boldsymbol{\omega}^* - \boldsymbol{\mu}_s|v, I\sigma_s^2).$$

The conditional prior distribution of v is also Gaussian due to the Z-distribution being a scale mixture Gaussian. \mathbf{v} is also a linear combination of $\mathbf{v}^* = (v_1^*, \dots, v_T^*)'$, where $v_1^* = v_1$ and $v_{t+1}^* = v_{t+1} - \phi v_t, t \geq 2$, conditionally independent Gaussian random variables:

$$f(v_1^*|\xi_1, \mu) = f(v_1|\xi_0, \mu) = \mathcal{N}(v_1^*|\mu, \frac{1}{\xi_0})$$

$$f(v_t^*|\xi_{t-1}, \mu, \phi) = f(v_t - \phi v_{t-1}|\xi_{t-1}, \mu, \phi) = \mathcal{N}(v_t^*|\mu(1 - \phi), \frac{1}{\xi_{t-1}}) \quad t \geq 2,$$

Similar to section B.2, we have:

$$f(\mathbf{v}|\boldsymbol{\xi}, \mu, \phi) = \mathcal{N}(\mathbf{v}|0, Q_{\boldsymbol{\xi}, \phi}^{-1}),$$

with

$$Q_{\xi, \phi} = \begin{bmatrix} \xi_1 + \phi^2 \xi_2 & -\phi \xi_2 & 0 & \dots & \dots & 0 \\ -\phi \xi_2 & \xi_2 + \phi^2 \xi_3 & -\phi \xi_3 & \ddots & \ddots & \vdots \\ 0 & -\phi \xi_3 & \xi_3 + \phi^2 \xi_4 & -\phi \xi_4 & \ddots & \\ \vdots & \ddots & \ddots & \ddots & \ddots & 0 \\ \vdots & \ddots & \ddots & -\phi \xi_{T-1} & \xi_{T-1} + \phi^2 \xi_T & -\phi \xi_T \\ 0 & \dots & \dots & 0 & -\phi \xi_T & \xi_T \end{bmatrix}$$

Thus,

$$f(\mathbf{v}|y^*, \dots) = \mathcal{N}\left(\mathbf{v} \mid \left(Q_{\xi, \phi} + I \frac{1}{\sigma_s^2}\right)^{-1} \left(\frac{\boldsymbol{\omega}^* - \mu_s}{\sigma_s^2} + Q_{\xi, \phi} \mathbf{1}\mu\right), \left(Q_{\xi, \phi} + I \frac{1}{\sigma_s^2}\right)^{-1}\right)$$

B.4 s

In section B.2, $\mathbf{s} = (s_1, \dots, s_T)'$ was introduced to expand $\boldsymbol{\omega}^*|\mathbf{v}$. Based on the same argument used in section B.1, $\forall k \in \{1, \dots, 10\}$

$$p(s_t = k | \omega_t^*, v_t) = \frac{\mathcal{N}(\omega_t^* | v_t + \mu_k, \sigma_k^2) p_k}{\sum_{i=1}^{10} p_i \mathcal{N}(\omega_t^* | v_t + \mu_i, \sigma_i^2)}, \quad \forall t \in \{1, \dots, T\}.$$

B.5 ξ

Based on Polson et al. [2013], we have

$$v_1 = \mu + \eta_0$$

$$v_t = \mu + \phi(v_{t-1} - \mu) + \eta_{t-1}, \quad \forall t \geq 2.$$

Naturally, $\eta_1 = v_1 - \mu$ and $\eta_t = v_{t+1} - \phi v_t - \mu(1 - \phi), \forall t \geq 2$.

$$f(\xi_0 | \mathbf{v}, \mu, \phi) = \mathcal{PG}(\xi_0 | 1, v_1 - \mu)$$

$$f(\xi_{t-1} | \mathbf{v}, \mu, \phi) = \mathcal{PG}(\xi_{t-1} | 1, v_t - \phi v_{t-1} - \mu(1 - \phi)) \quad \forall t \geq 2,$$

where \mathcal{PG} represents the density function for Polya-Gamma random variable.

B.6 μ

By the conditional independence, the likelihood reduces to the $\mathbf{v}^* | \boldsymbol{\xi}, \mu, \phi$, where the distribution of v^* discussed in Appendix B.3. To derive the conditional posterior for μ , let's consider $\hat{v}_\phi^* | \boldsymbol{\xi}, \mu, \phi := \frac{1}{T} \sum_{t=1}^T v_{\phi,t}^*$, where $v_\phi^* := [v_1^*, \frac{v_2^*}{(1-\phi)}, \dots, \frac{v_T^*}{(1-\phi)}]$. Indeed, we have

$$\begin{aligned} \hat{v}_\phi^* | \boldsymbol{\xi}, \mu, \phi &\sim N(\mu, \sigma_{\xi, \phi}^2) \\ \sigma_{\xi, \phi}^2 &:= \frac{1}{T^2} \left(\frac{1}{\xi_0} + \frac{1}{(1-\phi)^2} \sum_{t=1}^{T-1} \frac{1}{\xi_t} \right) \end{aligned}$$

The conditional prior distribution on μ also reduces to $f(\mu | \xi_\mu) = \mathcal{N}(\mu | 0, \frac{1}{\xi_\mu})$. Thus, the conditional posterior distribution for μ is

$$f(\mu | \hat{v}_\phi^*, \boldsymbol{\xi}, \xi_\mu, \phi) = \mathcal{N} \left(\mu \left| \left(\frac{1}{\sigma_{\xi, \phi}^2} + \xi_\mu \right)^{-1} \frac{\hat{v}_\phi^*}{\sigma_{\xi, \phi}^2}, \left(\frac{1}{\sigma_{\xi, \phi}^2} + \xi_\mu \right)^{-1} \right. \right).$$

B.7 ξ_μ

Based on the scale mixture representation of the Z-distribution Polson et al. [2013]:

$$f(\xi_\mu | \mu) = \mathcal{PG}(\xi_\mu | 1, \mu).$$

B.8 ϕ

Unlike other parameters, ϕ is not conditionally conjugate to its likelihood. Thus, the slice sampling method ? is used for the MCMC sampling. By taking the linear transformation of v_t , Let's consider its likelihood becomes $\hat{v}_\mu := \frac{1}{T-1} \sum_{t=2}^T v_{\mu,t}$, where $v_{\mu,t} = \frac{1}{2} \left(\frac{v_t - \mu}{v_{t-1} - \mu} + 1 \right)$.

We have the following conditional likelihood and prior for ϕ :

$$f(\hat{v}_\mu | \mu, \boldsymbol{\xi}) = \mathcal{N} \left(\hat{v}_\mu \left| \frac{\phi + 1}{2}, \frac{1}{(T-1)^2} \sum_{t=2}^T \frac{1}{4\xi_{t-1}(v_{t-1} - \mu)^2} \right. \right)$$
$$f\left(\frac{\phi + 1}{2}\right) \sim \text{Beta} \left(\frac{\phi + 1}{2} \left| 10, 2 \right. \right)$$